Collapse and revival oscillations as a probe for the tunneling amplitude in an ultra-cold Bose gas

Research Internship Report
Georgetown University, Washington D.C.
Feb 20 – Mai 20 2010
Supervisor: Prof. Dr. Marcos Rigol

Fabian Alexander Wolf

Note

This report is a documentation of the author's research internship with Prof. Marcos Rigol at Georgetown University, Feb 20 – Mai 20 2010. It consists of the Phys. Rev. A publication [1] and supplementary material. Sections 1, 3, 4, 5 and 6 are copies of the sections in the publication with the same name, except for references to the appendix and the correction of errors (see erratum below). The section 2 and the sections of the appendix are not present in the publication and provide detailed descriptions of methods and analytical calculations.

Erratum for Ref. [1]

During the production of this report the author (motivated by a remark of B. Sciolla) realized that two analytic expressions are not correctly given in the publication. None of the errors change any conclusion drawn in the publication, as well as all figures (and codes) are correct.

- In the analytic expression for the revival time (eq. (13) of the paper) a factor 2 in the second summand is incorrect. The corrected expression is given by:

$$t_{\mathrm{rev}} = \int_{u_1}^{u_2} \mathrm{d}u\, f(u), \quad \text{where} \quad f(u) = \left\{ d^2 J^2 (1-u^2)[1-(2\gamma-u)^2] - (\mathcal{H}_0' - Au)^2 \right\}^{-\frac{1}{2}}$$
$$\text{and} \quad \gamma = 2n-1 \quad \text{and} \quad \mathcal{H}_0' = -4n(1-n)\, d\, J - \gamma A.$$

- In the case of half filling, the constant A (in the publication always set 1) is missing in the expression for the upper boundary of the above integral. The correct expression is

$$u_2 = \frac{A}{2dJ} \left(\sqrt{1 + 8(\tfrac{dJ}{A})^2} - 1 \right) .$$

Abstract

We present a theoretical study of the quantum corrections to the revival time due to finite tunneling in the collapse and revival of matter wave interference after a quantum quench. We study hard-core bosons in a superlattice potential and the Bose-Hubbard model by means of exact numerical approaches and mean-field theory. We consider systems without and with a trapping potential present. We show that the quantum corrections to the revival time can be used to accurately determine the value of the hopping parameter in experiments with ultracold bosons in optical lattices.

Contents

1. Introduction

Collapse and revival oscillations in a Bose-Einstein condensate loaded in an optical lattice were first experimentally observed in 2002 [2] and since then have been a subject of much theoretical and experimental interest [3]. This phenomenon is understood as an oscillation between an initial coherent state and a final non-coherent (collapsed) state in a lattice where, after a quench, the hopping parameter between sites is negligible. Very recently it has been argued that such collapse and revival oscillations can be used as a very sensitive probe for effective three-body and higher interactions [6] by studying the time evolution of the visibility of the interference pattern. This has been investigated theoretically in Ref. [7]. It was assumed both in experiment and in theory [6, 7] that the initial state is a coherent state and that after the quench the tunneling amplitude is negligible, that is, that the systems were in the atomic limit. Following these assumptions, the time-evolving state is a product of coherent states localized at each lattice site and one deals with an effective one-site problem.

Our goal in this article is to go beyond the previous analysis and present a full many-body study of collapse and revival phenomena in one-, two-, and three-dimensional cubic lattices. We study hard-core bosons in the presence of a superlattice and the Bose-Hubbard model. For both cases we consider systems without and with a trapping potential present. For the hard-core case we use exact numerical approaches in one and two dimensions and compare them with the predictions of a Gutzwiller mean-field theory. We show that the latter is qualitatively and quantitatively correct when determining the revival time for small hopping amplitudes. Building on that, we present an analysis for the Bose-Hubbard model that is solely based on the Gutzwiller mean-field approach. We also provide an analytical solution for the homogeneous hard-core case.

A previous study [8] considered the effect of a finite hopping on the damping of the collapse and revival oscillations in a lattice without a confining potential. The quantitative results presented there applied to an initial coherent state as in the articles mentioned previously. In contrast, we study the dynamics starting from initial states that are the exact many-body ground state in some cases and the appropriate Gutzwiller ansatz in the other cases.

We find the functional form of those corrections to the revival time in the atomic limit, and show that if one knows the values of the superlattice potential for the hard-core case or the onsite interaction U for the Bose-Hubbard model, such corrections can be used to accurately determine the tunneling amplitudes in experiments in optical lattices. In the atomic limit, for the Bose-Hubbard model, the revival time $t_{\rm rev}$ is $t_{\rm rev}^{\rm atom} = 2\pi\hbar/U$ [4,5]. Our general strategy is to numerically calculate the deviations from this value for $0 < J/U < 1$. Given that in experiments with ultracold gases in optical lattices the hopping parameter J is exponentially sensitive to the lattice depth, while the onsite repulsion U is only power-law dependent on the lattice depth, this method of determining J by means of the revival time may be more accurate than the approaches followed so far. Our results are also relevant to cases in which the tunneling is small but one is still interested in estimating its value.

This report is organized as follows. In Sec. 2 the basic methods necessary to gain the results presented in the rest of the text are described. In Sec. 3, we study the collapse and revival in the hard-core case in the presence of a superlattice potential. This is done using numerically exact methods in one and two dimensions. In Sec. 4, we introduce the time-dependent mean-field approach to the hard-core boson problem and compare its results with numerically exact ones in order to quantify the predictive power of the mean-field approximation for the revival time. In addition, we make some general theoretical statements and provide an analytical solution for the case without the trapping potential. Section 5 is devoted to analyzing the Bose-Hubbard model in three dimensional systems of soft-core bosons with and without confining potentials present. Finally, we present our conclusions in Sec. 6.

2. Basic methods

2.1. Numerical exact time-evolution of hard-core bosons in one dimension

In the following we present an exact numerical approach to hard-core bosons (HCBs) in one dimension (1D) that was introduced by Rigol in Ref. [9]. This approach allows us to calculate the one particle Green's function with a numerical cost of L^5, L being the system size. Hence, it allows for calculations of systems that are comparable in size with experimentally realized ones - that is as much as several thousand lattice sites.

We start with the HCB system Hamiltonian that includes only a kinetic energy term. One accounts for the infinitely strong on-site repulsion by the prohibition of double occupancy implied by the operator constraint $\hat{b}_i^{\dagger 2} = \hat{b}_i^2 = 0$ for the creation and annihilation operator of the same site. Next neighbor summation in 1D reduces to the simple form below. J is the hopping parameter.

$$H_{\mathrm{HCB}} = -J \sum_i (b_i^\dagger b_{i+1} + \mathrm{h.\,c.})\,, \qquad \hat{b}_i^{\dagger 2} = \hat{b}_i^2 = 0\,, \qquad [b_i, b_j^\dagger] = \delta_{ij} \qquad [b_i, b_j] = [b_i^\dagger, b_j^\dagger] = 0\,. \quad (1)$$

2.1.1. Jordan-Wigner map on free fermions

The Hamiltonian (1) can be mapped on the equivalent Hamiltonian of free fermions, $H_{\mathrm{F}} = -J \sum_i (a_i^\dagger a_{i+1} + \mathrm{h.\,c.})\,,\ \{a_i, a_i^\dagger\} = \delta_{ij}\,,\ \{a_i, a_j\} = a_i^\dagger, a_j^\dagger = 0$, using the Jordan-Wigner transformation [10]:

$$b_j^\dagger = a_j^\dagger \prod_{\beta=1}^{j-1} e^{-i\pi a_\beta^\dagger a_\beta}\,. \quad (2)$$

Let us proof this proposition. One first shows that $a_i^\dagger, a_j$ obey the fermionic anti-commutation rules: We formally introduce for an arbitrary state $|\psi_{\mathrm{B}}\rangle$ of a HCB system the corresponding state of fermions $|\psi_{\mathrm{F}}\rangle$ with the same occupation numbers (which is possible as the bosonic state does not contain higher occupation numbers than 1). We further set without loss of generality

$i<j$ and denote with N_{0i} and N_{ij} the sums $\sum_\beta a_\beta^\dagger a_\beta$ over the sets of lattice sites $\{1,...,i-1\}$, $\{i+1,...,j-1\}$ respectively.

$$[b_i, b_j^\dagger] = \delta_{ij} \;\Rightarrow\; \Big[\prod_{\beta=1}^{i-1} e^{-i\pi a_\beta^\dagger a_\beta} a_i\,,\; a_j^\dagger \prod_{\gamma=1}^{j-1} e^{-i\pi a_\gamma^\dagger a_\gamma}\Big]|\psi_\mathrm{F}\rangle = \delta_{ij} \;\Rightarrow\; e^{i\pi N_{0i}}\Big[a_i\,,\; a_j^\dagger e^{i\pi a_i^\dagger a_i} e^{i\pi N_{ij}}\Big]|\psi_\mathrm{F}\rangle = \delta_{ij}$$
$$\Rightarrow\; \Big(a_i\, a_j^\dagger e^{-i\pi a_i^\dagger a_i} - a_j^\dagger e^{-i\pi a_i^\dagger a_i} a_i\Big)|\psi_\mathrm{F}\rangle = \delta_{ij} \;\Rightarrow\; \{a_i, a_j^\dagger\} = \delta_{ij}\,, \quad (3)$$

where in the second line it was used, that $e^{-i\pi a_i^\dagger a_i} a_i|\psi_\mathrm{F}\rangle = -a_i e^{-i\pi a_i^\dagger a_i}|\psi_\mathrm{F}\rangle$ (as site i in $|\psi_\mathrm{F}\rangle$ is either unoccupied or occupied with one particle). As $|\psi_\mathrm{F}\rangle$ is arbitrary the last arrow holds true. Analogously it can be shown that $\{a_i, a_j\} = \{a_i^\dagger, a_j^\dagger\} = 0$.

It remains to show that the form of the Hamiltonian is not change by the Jordan-Wigner map. For this insert (2) in (1):

$$H_\mathrm{HCB} = -J\sum_i (a_i^\dagger \underbrace{\prod_{\beta=1}^{i-1} e^{-i\pi a_\beta^\dagger a_\beta} \prod_{\gamma=1}^{i} e^{i\pi a_\gamma^\dagger a_\gamma}}_{e^{i\pi n_i}=1} a_{i+1} + \mathrm{h.\,c.}) = H_\mathrm{F}\,. \quad (4)$$

The identity under the brace holds true, because $\langle\psi_\mathrm{F}|a_i^\dagger e^{-i\pi n_i}$ can only yield $n_i = 0$, as double occupation in $\langle\psi_\mathrm{F}|$ is forbidden.

A last thought has to be given to the boundary conditions. Let's clear up the case for periodic ones. For an electron at site 1 the processes to hop from site N by passing the boundary or performing commutations with all other electrons on the lattice sites in between should be equivalent. For an even total number of electrons N there is an odd number to commute with - to make up for this, one adds an additional minus sign to the hopping constant of process $1 \to N$. For an odd number this does not occur and one can leave everything unchanged.

With this mapping we now possess a tool to easily calculate exact quantities - we no more deal with a strongly-interacting bosonic system but with a simple non-interacting fermionic one. This fact makes it eventually possible to trivially extend our analysis to the nonequilibrium case.

2.1.2. Time evolution of free fermions

The state $|\Psi_\mathrm{F}\rangle$ of a noninteracting system is a product of single particle states $|\psi_n\rangle$. The real space representation of a single particle state is a superposition of occupation amplitudes for each site of the lattice, which leaves us with

$$|\Psi_\mathrm{F}\rangle = |\psi_1\rangle \otimes ... \otimes |\psi_N\rangle\,, \qquad |\psi_n\rangle = \sum_{i=1}^{L} a_i^\dagger\, P_{in}\,|0\rangle\,, \quad (5)$$

where the coefficients P_{in} fulfill $\sum_{i=1}^L P_{in}^2 = 1$ (such that $\langle\psi_n|\sum_{i=1}^L n_i|\psi_n\rangle = 1$). We introduce the matrix $\boldsymbol{P}$ of coefficients ($\boldsymbol{P}_n$ denotes the vector in the nth column) and the vector of operators

$\boldsymbol{a}^\dagger = (a_1^\dagger, ..., a_L^\dagger)$ and summarize:

$$|\Psi_\mathrm{F}\rangle = \prod_{n=1}^{N} \sum_{i=1}^{L} (a_i^\dagger P_{in})|0\rangle = \prod_{n=1}^{N} \boldsymbol{a}^\dagger \boldsymbol{P}_n |0\rangle \,. \tag{6}$$

One can now give an easy expression for the action of a quadratic exponential on $|\Psi_\mathrm{F}\rangle$ [11].

Proposition. Given the above definitions the following identity holds true for any hermitian $L \times L$ matrix $\boldsymbol{X}$

$$e^{\boldsymbol{a}^\dagger \boldsymbol{X} \boldsymbol{a}} \prod_{n=1}^{N} \boldsymbol{a}^\dagger \boldsymbol{P}_n |0\rangle = \prod_{n=1}^{N} \boldsymbol{a}^\dagger \left(e^{\boldsymbol{X}} \boldsymbol{P}\right)_n |0\rangle \,. \tag{7}$$

Proof. See Ref. [11].

In our case, we use this proposition for $e^{\boldsymbol{a}^\dagger \boldsymbol{X} \boldsymbol{a}} \equiv \prod_{\beta=1}^{j-1} e^{-i\pi a_\beta^\dagger a_\beta}$, i.e. the map of the Jordan-Wigner transformation, and for $e^{\boldsymbol{a}^\dagger \boldsymbol{X} \boldsymbol{a}} \equiv e^{iH_\mathrm{F} t}$, i.e. the time evolution propagator of the free fermionic system. In the latter case the proposition is just a mathematical notation of the fact that the overall evolution of a non-interacting system is equivalent to the product of the independently evolving single-particle states.

This allows us to choose a representation of H_F in the L-dimensional space of single particle states $|\psi_n\rangle = \sum_{i=1}^{L} a_i^\dagger P_{in} |0\rangle$. With this it is clear that we do not have to perform any calculation in an $\binom{L}{N}$-dimensional, i.e. exponentially large, space of a manybody states.

As an example and for comparison with later results, we compute the one-particle density matrix for non-interacting fermions ρ_{ij}. First we evaluate

$$a_j |\Psi_\mathrm{F}\rangle = a_j \prod_{n=1}^{N} \sum_{\beta=1}^{L} (a_\beta^\dagger P_{\beta n})|0\rangle = \left(P_{j1} - \sum_{\gamma=1}^{L} a_\gamma^\dagger P_{\gamma 1}\, a_j\right) \prod_{n=2}^{N} \sum_{\beta=1}^{L} (a_\beta^\dagger P_{\beta n})|0\rangle \tag{8}$$

We further note that all expressions of the form below vanish:

$$\underbrace{\langle 0| \prod_{m=c}^{N} \sum_{\delta=1}^{L} (P_{\delta m}^\dagger a_\delta) \sum_{\gamma=1}^{L} (a_\gamma^\dagger P_{\gamma 1})}_{\text{state of } (N-c+1) \text{ particles}} \; a_j \underbrace{\prod_{n=c+1}^{L} \sum_{\beta=1}^{L} (a_\beta^\dagger P_{\beta n})|0\rangle}_{\text{state of } (N-c-1) \text{ particles}} = 0 \,, \tag{9}$$

where further action of operator a_j to the right makes the unbalanced situation in terms of particle numbers worse (see (8)). States with different particle numbers are orthogonal, such that all terms yield zero.

Application of (8) and (9) to the line below, and from then in a successive way yields the

result:

$$\rho_{ij} = \langle \Psi_{\rm F}| a_i^\dagger a_j |\Psi_{\rm F}\rangle$$
$$= P_{i1}^\dagger P_{j1} + \langle 0| \prod_{m=c}^{N} \sum_{\delta=1}^{L} (P_{\delta m}^\dagger a_\delta)\; a_i^\dagger \underbrace{\sum_{\epsilon=1}^{L} (P_{\epsilon 1}^\dagger a_\epsilon) \sum_{\gamma=1}^{L} (a_\gamma^\dagger P_{\gamma 1})}_{\langle\psi_1|\psi_1\rangle=1}\; a_j \prod_{n=c+1}^{L} \sum_{\beta=1}^{L} (a_\beta^\dagger P_{\beta n})|0\rangle \tag{10}$$
$$= \sum_n P_{in}^\dagger P_{jn} \tag{11}$$

2.1.3. Time evolution of hard-core bosons

To treat HCBs in an effective way we employ the Jordan Wigner transformation and perform the following formal steps (this proceeding can be found in the brief review [9]). The time evolution of the Green's function is:

$$G_{ij}(t) = \langle \Psi_{\rm B}(t)| b_i b_j^\dagger |\Psi_{\rm B}(t)\rangle \;= \langle \Psi_{\rm F}(t)| \prod_{\delta=1}^{i-1} e^{i\pi a_\delta^\dagger a_\delta}\;\; a_i\, a_j^\dagger \prod_{\epsilon=1}^{j-1} e^{-i\pi a_\epsilon^\dagger a_\epsilon} |\Psi_{\rm F}(t)\rangle \tag{12}$$

The time evolution of the fermionic state $\Psi_{\rm F}$ is trivial following (7)

$$|\Psi_{\rm F}(t)\rangle = e^{-iH_{\rm F}t}|\Psi_{\rm F\,init}\rangle = \prod_{n=1}^{N} \boldsymbol{a}^\dagger \boldsymbol{P}_n(t)|0\rangle\,, \qquad \boldsymbol{P}_n(t) = (e^{-iH_{\rm F}t}\boldsymbol{P}_0)_n \tag{13}$$

Once it is calculated the action of $\prod_{\epsilon=1}^{j-1} e^{-i\pi a_\epsilon^\dagger a_\epsilon}$ on $|\Psi_{\rm F}(t)\rangle$ in (12) generates only a sign change on the elements $P_{\beta n}$ for $\beta \leq j-1$. The further action of $a_j^\dagger$ – the generation of a particle – corresponds to an addition of one column to $\boldsymbol{P}(t)$ with elements $P_{\beta(N+1)} = \delta_{\beta j}$. This map we denote with $\boldsymbol{P} \to \boldsymbol{P}^j$. Hence, the HCB Green's function is obtained as

$$G_{ij}(t) = \langle 0| \prod_{m=1}^{N+1} \sum_{\alpha=1}^{L} P_{\alpha m}^i a_\alpha \;\; \prod_{n=1}^{N+1} \sum_{\beta=1}^{L} a_\beta^\dagger P_{\beta n}^j |0\rangle$$
$$= \det\left(\boldsymbol{P}^{i\,\dagger} \boldsymbol{P}^j\right), \tag{14}$$

because

$$\langle 0| a_{\alpha_1} ... \, a_{\alpha_{N+1}} a_{\beta_{N+1}}^\dagger ... \, a_{\beta_1}^\dagger |0\rangle = \epsilon^{\lambda_1 ... \lambda_{N+1}}\; \delta_{\alpha_1\beta_{\lambda_1}} ... \, \delta_{\alpha_{N+1}\beta_{\lambda_{N+1}}}\,. \tag{15}$$

We then get the one particle density matrix with

$$\rho_{ij}(t) = \langle \Psi_{\rm B}(t)| b_i^\dagger b_j |\Psi_{\rm B}(t)\rangle = G_{ji}(t) + \delta_{ij}(1 - 2G_{ii}(t))\,, \tag{16}$$

and the momentum distribution function as

$$n_k(t) = \frac{1}{A} \sum_{jl} e^{-ik(j-l)} \rho_{jl}(t)\,, \tag{17}$$

with a constant A (in the homogeneous case we set, as usual, $A = L$).

We finally calculate the numerical cost for a calculation of a time step, given we already diagonalized the Hamiltonian in its single particle real space representation (this has to be done only once at the beginning and costs L^3). We have L^2 operations for the matrix product in (14) and L^3 for the calculation of the determinant in (14) (using a LR decomposition) – giving us L^5. The code used by the author was observed to scale with an exponent of 4.8 with respect to the system size, reflecting the L^5 result.

2.2. Quantum particles in a harmonic trap

2.2.1. The characteristic density

The Hamiltonian of the Bose-Hubbard model (although the following thoughts will not distinguish between bosons and fermions) in a harmonic trap is the following

$$H_{\mathrm{HCB}} = -J \sum_{\langle ij \rangle} (b_i^\dagger b_j + \mathrm{h.\,c.}) + \frac{U}{2} \sum_i n_i(n_i - 1) + V \sum_i r_i^2 n_i \,, \tag{18}$$

where r_i denotes the distance from the minimum of the trap in units of the lattice spacing a. In one dimension e.g. we have $r_i = a\, i$ where i is the site index with $i \in [-\frac{N}{2}, \frac{N}{2}]$.

To reduce the number of parameters and to make arguments more clear, we first consider the case of HCBs in one dimension. In the case without a trap, i.e. again the Hamiltonian (1) it is obvious that the hopping constant J only sets the energy scale but has no further influence on the physical properties of the system. One therefore states that the density $\rho = \frac{N}{L}$ completely determines these physical properties [12].

We now interpret the density as the ratio of the 'required' and 'available' space in the 1D system: $\rho = \frac{N}{L} = \frac{Na}{La}$, that is the 'confinement' of the particles in the system (we can use the expression 'confinement' as particles repel each other). Applying an harmonic external potential naturally constitutes a confinement regardless of the number of particles by locating particles in a neighborhood of the minimum of the trapping potential. Even with only a few particles in the system, the density on a single site can rise up to 1 and therefore make the system a Mott insulator - if only the trap is steep enough. The density ρ does of course not account for that such that one has to find a different characteristic quantity.

In order to find the appropriate length scale measuring the 'available' space for the particles in the system we rewrite the 1D HCB Hamiltonian in a dimensionless effective way (i.e. we get rid of one redundant parameter):

$$H_{\mathrm{HCB}}/J = -\sum_i (b_i^\dagger b_{i+1} + \mathrm{h.\,c.}) + \sum_i \Big(\frac{r_i}{\sqrt{J/V}}\Big)^2 n_i \,. \tag{19}$$

This notation gives rise to the scale $\zeta = \sqrt{(J/V)}\, a$ that is obviously meaningful: The bigger the curvature of the trap, the more located are particles; the bigger the hopping parameter, the less located are particles. Occupation probability is proportional to the energy cost which is

proportional to the square of the distance from the minimum of trap - therefore we take the root of J/V. If we again consider the 'required' space Na and calculate the ratio with ζ we end up with the characteristic density of the system [13]:

$$\tilde{\rho} \equiv N\sqrt{\frac{V}{J}}\,. \tag{20}$$

In the case of higher dimensions we have to account for the fact that distances are measured as the Dth root of the volume when D is the dimension. Of course the 'required' space is then a general volume Na^D (dependent on the volume per lattice site a^D). On the other hand the argumentation for the length scale of the 'available space' still holds true such that it can be given as ζ^D. The ratio is then

$$\tilde{\rho}_D \equiv N\left(\frac{V}{D\,J}\right)^{\frac{D}{2}}\,. \tag{21}$$

Although all argumentation was made for HCBs, it still obviously holds true for a system with a fixed finite repulsion U – apart from that U enters the Hamiltonian as a second (effective) parameter that governs the localization of particles.

2.2.2. Example: Expansion of a trapped hard-core boson cloud

At this point we can already give the interesting application of the free expansion of HCBs using only the so far discussed methods (a brief review is found in [9]). One prepares a system of trapped bosons in their ground state that is (depending only on the characteristic density) either a quasi-condensate (quasi-superfluid) or a Mott insulator, and then removes the harmonic trapping potential in order to let the particle cloud expand. In the first case [12] one finds an expansion during which the peaked initial momentum distribution of the HCBs approaches that of fermions in their ground state (Fermi block). However the lowest natural orbital occupation (i.e. the biggest eigenvalue of the one particle density matrix) rises, which means that the system remains a quasi condensate at all times and does not loose coherence. In the second case [14], opposed to that, starting from a flat (Mott insulator) momentum distribution a quasi condensate with peaks at finite momentum is building up - in three dimensions this phenomenon of a coherent traveling atom cloud has recently been proposed to be a first proof of principle of a matter laser [15].

3. Numerically exact results for hard-core bosons in a superlattice

We first introduce the model Hamiltonian considered to study hard-core bosons in a superlattice. We also discuss its relation to the interaction quench in the soft-core case that is studied in Sec. 5.

3.1. Motivation and methods

The hard-core boson Hamiltonian on a superlattice with period 2 in the presence of a harmonic confining potential can be written as

$$\hat{H}_{\rm HCB} = -J \sum_{\langle ij \rangle} \left(\hat{b}_i^\dagger \hat{b}_j + {\rm H.c.} \right) + A \sum_i (-1)^i \hat{n}_i + V \sum_i r_i^2 \hat{n}_i \,, \tag{22}$$

where the hard-core creation and annihilation operators at site i are denoted by $\hat{b}_i^\dagger$ and $\hat{b}_i$, respectively, and the local density operator by $\hat{n}_i = \hat{b}_i^\dagger \hat{b}_i$. Hard-core boson operators satisfy standard commutation relations for bosons. However, on the same site, they also satisfy the constraint $\hat{b}_i^{\dagger 2} = \hat{b}_i^2 = 0$, which precludes multiple occupancy of the lattice sites. The other parameters in Eq. (22) are the hopping constant J between nearest-neighbor sites $\langle ij \rangle$, the strength of the superlattice potential A, and the curvature of the harmonic trap V. The distance from site i to the center of the trap r_i is measured in units of the lattice constant a, which we set to unity. In what follows, we also denote the total number of lattice sites by L and the total number of particles by N.

The hard-core model on a superlattice is particularly suitable to study collapse and revival phenomena because in one dimension (1D) it can be exactly solved by means of the Jordan-Wigner mapping to noninteracting fermions [10]. In equilibrium, these systems were studied in Ref. [16], where they were shown to exhibit ground state phases that are similar to those of the Bose-Hubbard model. The nonequilibrium dynamics of hard-core bosons in a superlattice potential was studied in Ref. [17], where collapse and revival oscillations of the momentum distribution function were observed.

A quench of the superlattice potential A in Eq. (22) has a similar effect to a quench of U in the Bose-Hubbard model. From a simple band-structure calculation it follows that in 1D A opens a gap $\Gamma = 2A$ in the hard-core boson energy spectrum [16, 17],

$$\epsilon_\pm(k) = \pm \sqrt{4J^2 \cos^2(ka) + A^2} \,, \tag{23}$$

where "+" ("−") denotes the upper (lower) band. In two (2D) and three (3D) dimensions, hard-core bosons cannot be mapped to noninteracting fermions. The phase diagrams for the ground state of such systems were studied in detail in Refs. [18, 19] by various numerical and analytical approaches, and were shown to be qualitatively similar to the phase diagrams of the Bose-Hubbard model in 2D and 3D [20–22].

As already noted, in the atomic limit of the Bose-Hubbard model, the revival time after the interaction quench is given by $t_{\rm rev}^{\rm atom} = 2\pi/U$ (we set $\hbar \equiv 1$ henceforth); similarly, for hard-core bosons in a superlattice potential, it follows that $t_{\rm rev}^{\rm atom} = \pi/A$ [17].

Hence, in this section we take advantage of the fact that the nonequilibrium dynamics of hard-core bosons in 1D can be exactly solved for large system sizes by means of the approach presented in Refs. [9], which makes use of the Jordan-Wigner transformation to noninteracting

fermions [10]. In 2D, due to the reduced Hilbert space (when compared to soft-core bosons), one can perform full diagonalization calculations for small, but meaningful, periodic systems. All our exact results for 2D hard-core systems were obtained in 4×4 lattices with periodic boundary conditions.

The two preceding approaches allow us to make exact predictions for the quantum corrections due to finite hopping amplitudes to the revival time $t_{\rm rev}^{\rm atom}$

$$\Delta t_{\rm rev} = t_{\rm rev}^{\rm atom} - t_{\rm rev}, \tag{24}$$

which in turn will help us gauge the accuracy of the mean-field approach that we use later for studying the Bose-Hubbard model.

In the latest experimental and theoretical studies [6, 7], the main observable under consideration was the visibility of the interference pattern. Here, instead, we focus our attention on the time evolution of the $n_{k=0}$ momentum occupation number,

$$n_{k=0} = \frac{1}{L} \sum_{ij} \langle \hat{b}_i^\dagger \hat{b}_j \rangle, \tag{25}$$

which is also measured in experiments.

3.2. Results for hard-core bosons in a periodic potential in 1D and 2D

In all cases for hard-core bosons presented here we consider the following quench. A system is prepared in a superfluid state with $J_{\rm ini} = 1$ (which sets our energy scale) and no superlattice potential. At time $t = 0$ the superlattice potential A is quenched to a constant value $A_{\rm fin} = 1$ and the hopping constant J is reduced to several values $J_{\rm fin} < 1$ (in the remainder of the text, the notation $A_{\rm fin} \equiv A$ and $J_{\rm fin} \equiv J$ is used in all unambiguous cases).

In Fig. 1, we show the time evolution of $n_{k=0}$ after this quench in (a) a chain and (b) a 4×4 cluster, both at quarter filling. Results are presented for three different final values of J, where the atomic limit ($J = 0$) revival time can be clearly seen to correspond with the prediction $t_{\rm rev}^{\rm atom} = \pi/A$. Two effects of finite final hopping are evident in those plots: first, a clear shift in the frequency of the oscillations and, second, a damping of the amplitude. In the following, we restrict our analysis to the period and amplitude of the first revival. In the homogeneous case, the frequency can be calculated from the revival time. In the presence of a confining potential, this is in general not possible as the exact revival time can change on long time scales.

The quantum corrections due to finite hopping $\Delta t_{\rm rev}$ versus J for constant $A = 1$ are presented in a log-log plot in Fig. 2(a) for 1D and 2D systems. We find from those plots that the corrections follow a quadratic behavior for values of $J \lesssim 0.1$. This is depicted by a quadratic fit $f(x) = ax^2$ to data points with $J \leq 0.01$. Also evident from those plots is the very weak dependence of $\Delta t_{\rm rev}$ on the density both in 1D and 2D. This turns out to be very convenient later when studying the harmonically trapped systems.

In Fig. 2(b) we consider the damping of the oscillations, which can be characterized by the

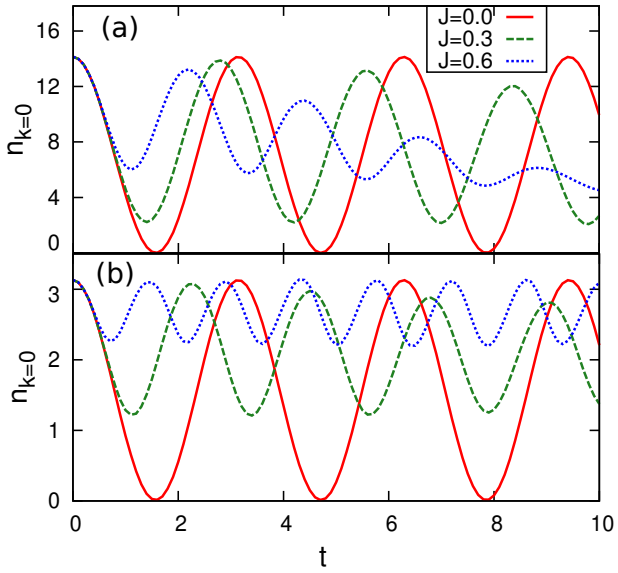

Figure 1: (Color online) Time evolution of $n_{k=0}(t)$ for three final values for the hopping constant, $J_{\rm fin} = 0$, $J_{\rm fin} = 0.3$, and $J_{\rm fin} = 0.6$, in a system with a superlattice potential in 1D (a) and 2D (b). These calculations were done in a chain with $L = 400$ lattice sites in 1D and in a $L = 4 \times 4$ system in 2D, both at quarter filling. Time is measured in units of $\hbar/J_{\rm ini}$.

amplitude of the first revival $n^{\rm rev}_{k=0} = n_{k=0}(t = t_{\rm rev})$ subtracted from its value in the atomic limit: $\Delta n^{\rm rev}_{k=0} = n^{\rm atom,rev}_{k=0} - n^{\rm rev}_{k=0}$. For this quantity we find a quartic behavior, as illustrated by the fits in Fig. 2(b) and a much stronger dependence on the density. The very fast reduction of the damping with decreasing J makes it a less attractive tool for experimentally probing small values of J.

We find numerically the scaling of $t_{\rm rev}$ with respect to the system parameters J and A to have the following functional form $t_{\rm rev}(J, A) \equiv t_{\rm rev}(J/A)/A$ whereas for the damping $n^{\rm rev}_{k=0}(J, A) \equiv n^{\rm rev}_{k=0}(J/A)$; that is, the former depends on the value of A and J/A while the latter is only a function of the ratio J/A. In the atomic limit, the revival time scales with A: $t^{\rm atom}_{\rm rev}(A) = \pi/A$ and therefore the preceding scaling holds also true for $\Delta t_{\rm rev}$: $\Delta t_{\rm rev}(t, A) \equiv \Delta t_{\rm rev}(t/A)/A$. In Sec. 4 we are able to analytically confirm this result for the mean-field approximation. On the other hand, in the atomic limit, $n^{\rm max}_{k=0}(A)$ is independent of A as the system exhibits perfect revivals so $\Delta n^{\rm rev}_{k=0}$ is only a function of J/A.

3.3. Results for hard-core bosons in a trap in 1D

Experimental systems are in general different from the ones discussed in Sec. 3.2. This is because a confining potential is required for containing the gas of bosons. The confining potential in experiments is to a good approximation harmonic, and generates an inhomogeneous density profile. Given the results shown in Fig. 2(a), where the revival time was shown to depend only weakly on the density, one would expect the outcome in the presence of a trap not to be strongly dependent on the confining potential and the total number of particles.

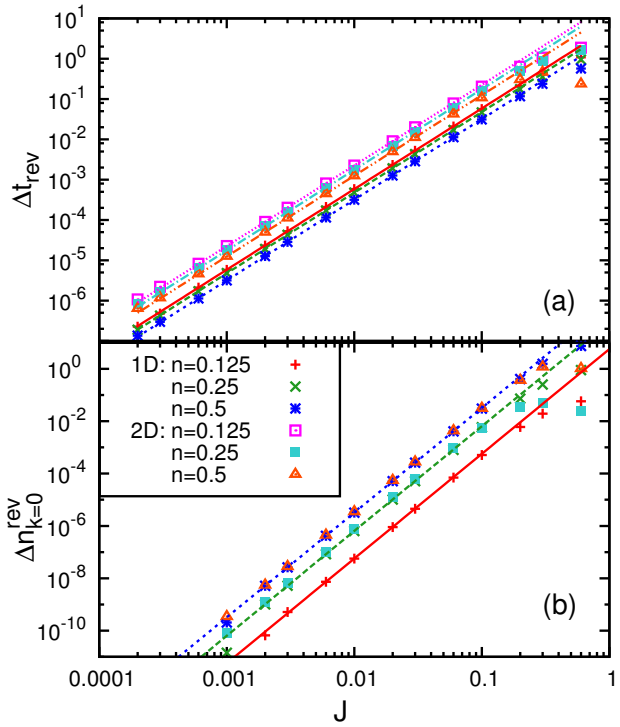

Figure 2: (Color online) Quantum corrections to (a) the revival time ($\Delta t_{\rm rev}$), and (b) the revival amplitude ($\Delta n^{\rm rev}_{k=0}$), vs J. Results are presented for three densities $n = 0.125$, $n = 0.25$ and $n = 0.5$ in 1D and 2D. In (a) a quadratic dependence is observed whereas in (b) a quartic dependence is present. These behaviors are emphasized by power-law fits for data points with $J \leq 0.01$. The system sizes for 1D are $L = 800$ for $n = 0.125$, and $L = 400$ for $n = 0.25$ and $n = 0.5$, and for 2D $L = 4 \times 4$ for all densities. Results for $n > 0.5$ trivially follow from the particle-hole symmetry of the model. No data are presented for $n = 0.125$ in (b) because only two particles are present in the 4×4 cluster and no damping occurs.

Up to small corrections, the preceding turns out to be the case for the changes induced in the revival time by a finite hopping. However, as shown in Fig. 3(a), if one quenches J and A keeping constant the trapping potential, then a very high damping rate can be seen even in the atomic limit. Hence, measurements at a constant curvature of the trap are not the best way to proceed in trapped systems. They mix the effects of the trapping potential and the finite hopping in the outcome. In fact, even the quadratic behavior obvious in the homogeneous case (Fig. 2) becomes obscured in the trap if the confining potential is kept the same from the initial state.

In previous work in equilibrium it has been argued that the correct way to define the thermodynamic limit for a trapped system is by keeping constant the so-called characteristic density $\tilde{\rho} = N[V/(dJ)]^{\frac{d}{2}}$, where d is the dimensionality of the system (see, e.g., Ref. [23]). This is equivalent to what is done in homogeneous systems when one keeps constant the density N/L. Since in Sec. 3.2 all quenches were performed keeping constant N/L, we have studied quenches in the trap in which the characteristic density is kept constant; that is, one needs to reduce

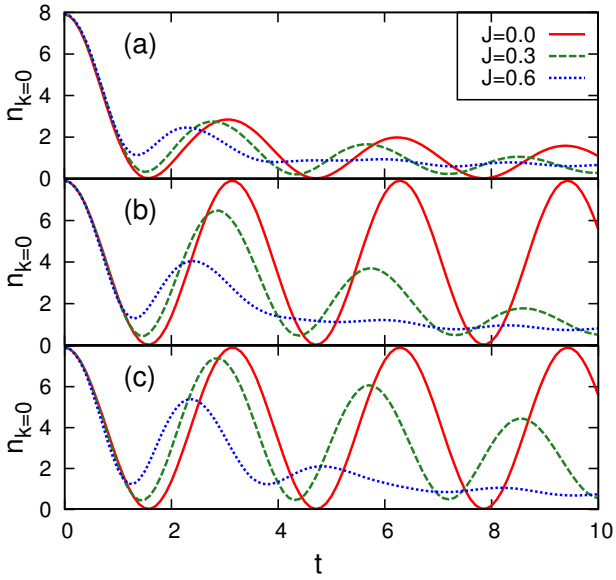

Figure 3: (Color online) Time evolution of $n_{k=0}(t)$ in a trap after a quench with (a) constant curvature $V = 10^{-4}$, (b) constant characteristic density $\tilde{\rho} = 1.0$, and (c) turning off the trap ($V_{\rm fin} = 0$), all for the same initial state. In text (b) and (c) are referred to as quench type (i) and (ii), respectively. These calculations were done for a system with $L = 400$ and $N = 100$. To keep the characteristic density constant during the quench we changed $V_{\rm ini} = 10^{-4} \to V_{\rm fin} = 0$ for $J = 0$, $V_{\rm ini} = 10^{-4} \to V_{\rm fin} = 3 \times 10^{-5}$ for $J = 0.3$ and $V_{\rm ini} = 10^{-4} \to V_{\rm fin} = 6 \times 10^{-5}$ for $J = 0.6$.

the trapping potential by the same amount that the hopping parameter is reduced. We denote this scenario quench type (i). Another way of reproducing the homogeneous results that comes to mind is to remove the trapping potential concurrently with the superlattice quench and observe oscillations which then take place in a homogeneous potential. This scenario is denoted quench type (ii). Within the second approach, one realizes that the gas starts expanding after the quench. However, if the considered hopping parameters and revival times are sufficiently small, this will not constitute a problem. Results for the dynamics of these cases are shown in Figs. 3(b) and 3(c). In contrast to the quench that keeps constant the curvature of the trap we now observe that the time evolution of $n_{k=0}$ is very similar to the one in homogeneous systems depicted in Fig. 1.

For both quench scenarios (i) and (ii), we find a quadratic behavior for $\Delta t_{\rm rev}$, which is similar to what was shown in Fig. 2 for homogeneous systems. Interestingly this behavior is, as depicted in Fig. 4(a), practically independent of the quench type and the characteristic density of the initial state. We note that for $\tilde{\rho} = 3.0$ the initial state has an insulating ($n = 1$) domain in the center of the trap, while for the other characteristic densities the system is purely superfluid. In 1D, the insulator appears in the center of the trap when $\tilde{\rho} \sim 2.6 - 2.7$ [9]. The independence of the asymptotic behavior of $\Delta t_{\rm rev}$ on the initial state suggests that by measuring the correction to the revival time due to the finite value of J in experiments, it is possible to determine J if one knows A. The same can be said for systems without a trap.

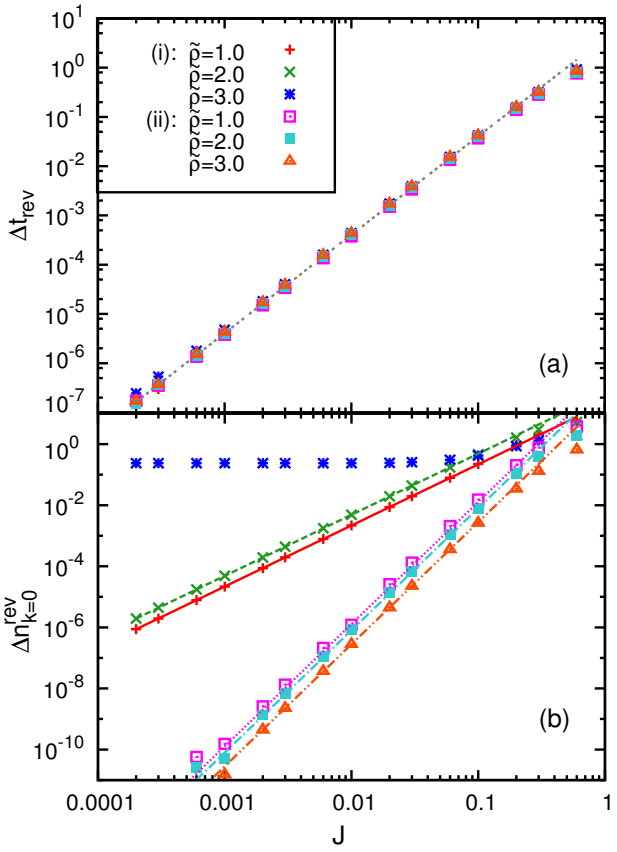

Figure 4: (Color online) Quantum corrections to (a) the revival time ($\Delta t_{\rm rev}$), and (b) the revival amplitude ($\Delta n^{\rm rev}_{k=0}$) vs J for $A_{\rm fin} = 1$, both for the quench scenarios (i) keeping the characteristic density constant, and (ii) turning off the trap. Results are presented for three different initial values of the characteristic density $\tilde{\rho} = 1.0$, $\tilde{\rho} = 2.0$, and $\tilde{\rho} = 3.0$, which correspond to curvatures $V_{\rm ini} = 4.44 \times 10^{-5}$, $V_{\rm ini} = 1.78 \times 10^{-4}$, and $V_{\rm ini} = 4 \times 10^{-4}$, respectively; the system sizes are $L = 500$, $L = 400$, $L = 300$, with $N = 150$ in all cases. Note that $\tilde{\rho} = 3.0$ already has a Mott-insulating region in the center of the trap, while $\tilde{\rho} = 1.0$ and $\tilde{\rho} = 2.0$ are entirely superfluid. The quadratic and quartic fits in (a) and (b) were done for points with $J \leq 0.01$.

On the other hand, as shown in Fig. 4(b), $\Delta n^{\rm rev}_{k=0}$ reveals a strong dependence on the quench type and the initial density. For scenario (i), we obtain a quadratic behavior for pure superfluid initial states ($\tilde{\rho} = 1.0$ and $\tilde{\rho} = 2.0$), while for the one having a Mott insulating domain ($\tilde{\rho} = 3.0$) a constant damping rate is always present for $J < 1$. For quench type (ii), the damping behaves completely differently and shows the quartic behavior observed in the homogeneous case. With respect to the aim to simulate the homogeneous case, this result indicates that the fact that the density profile remains unchanged during the time evolution under scenario (i) is less important than the fact that the potential is homogeneous after quench (ii).

4. Mean-field approach

Within the mean-field approximation, we can extend our analysis to consider the more experimentally relevant Bose-Hubbard model:

$$\hat{H}_{\mathrm{SCB}} = -J \sum_{\langle ij \rangle} (\hat{a}_i^\dagger \hat{a}_j + \mathrm{H.\,c.}) + \frac{U}{2} \sum_i \hat{n}_i (\hat{n}_i - 1) + \sum_i \hat{n}_i V r_i^2 \,, \tag{26}$$

where $[\hat{a}_i, \hat{a}_j^\dagger] = \delta_{ij}$ and $[\hat{a}_i, \hat{a}_j] = [\hat{a}_i^\dagger, \hat{a}_j^\dagger] = 0$, as usual for bosons. The on-site interaction energy is denoted by U.

The mean-field theory that we employ is based on the restriction of the wave function to the Gutzwiller-type product state,

$$|\Psi_{\mathrm{MF}}\rangle = \prod_{i=1}^{L} \sum_{n=0}^{n_{\mathrm{c}}} \alpha_{in} |n\rangle_i \,, \tag{27}$$

where $n_{\mathrm{c}} \to \infty$ for thermodynamic systems, $|n\rangle_i$ denotes a single-site Fock state for lattice site i and the complex coefficients α_{in} allow for a time dependence. For all numerical calculations, a finite cutoff n_{c} is taken.

The mean-field ground state in equilibrium is found by minimization of the energy expectation value,

$$\langle \Psi_{\mathrm{MF}} | \hat{H}_{\mathrm{SCB}} - \mu \hat{N} | \Psi_{\mathrm{MF}} \rangle, \tag{28}$$

where μ is the chemical potential and $\hat{N}$ counts the total number of particles. Hence, from here on we work on the grand-canonical ensemble. To find the time-evolution of the mean-field approximated system, we employ the time-dependent variational principle [24] that minimizes the expression

$$\langle \Psi_{\mathrm{MF}} | i\partial_t - \hat{H}_{\mathrm{SCB}} + \mu \hat{N} | \Psi_{\mathrm{MF}} \rangle \,, \tag{29}$$

and yields the following set of differential equations (for the derivation see appendix A):

$$i\dot{\alpha}_{in} = -J \sum_{\langle j \rangle_i} \left(\sqrt{n+1}\, \alpha_{i(n+1)} \Phi_j^* + \sqrt{n}\, \alpha_{i(n-1)} \Phi_j \right) + \alpha_{in}\, n \left[\frac{U}{2}(n-1) + V r_i^2 - \mu \right] . \tag{30}$$

Here $\Phi_j = \langle a_j \rangle = \sum_{n=1}^{n_{\mathrm{c}}} \sqrt{n}\, \alpha_{j(n-1)}^* \alpha_{jn}$, $\alpha_{i(-1)} = \alpha_{i(n_{\mathrm{c}}+1)} = 0$, and $\sum_{\langle j \rangle_i}$ denotes summation over all j that are nearest neighbors of i. This is a set of $L \times n_{\mathrm{c}}$ equations. The time evolution described by Eq. (30) preserves normalization and the total particle number N. We solve the system numerically using a fourth-order Runge-Kutta method. Self-consistency is guaranteed by monitoring the total energy, particle number, and normalization.

At this point it is important to stress that this mean-field approach is in principle an uncontrolled approximation. We gauge its validity against our exact results in Sec. 4.2. Before doing so, we present an instructive analytical solution for the equations introduced previously in the hard-core limit and for a periodic potential ($V = 0$).

4.1. Analytical mean-field solution for hard-core bosons in a periodic potential

In the case of hard-core bosons, it is possible to reduce the number of equations considerably and employ a parametrization for the α_{in} in Eq. (30) that preserves normalization and deals with real variables – this is due to the equivalence of hard-core bosons to $s = 1/2$ spins, which leads to the following ansatz for the Gutzwiller wave function [25]:

$$|\Psi_{\mathrm{HCB}}\rangle = \prod_{i=1}^{L} \mathrm{e}^{i\chi_i} \left(\sin\frac{\theta_i}{2} + \cos\frac{\theta_i}{2} \mathrm{e}^{i\phi_i} a_i^\dagger \right) |0\rangle \,. \tag{31}$$

If there is no trap in the system ($V = 0$) it is possible to use translational invariance to simplify the equations (30), in which in the hard-core limit we again employ the superlattice quench introduced before. This leads to a formal replacement of $U(n-1)/2$ by A in (30). As all sites with the same potential must have the same properties and the system's wavefunction is a product of single-site states, the L-site system can be reduced to an effective two-site problem (for two on-site potentials $\mu_{1/2} = \mu \pm A$) independent of the dimension. Then the ansatz Eq. (31) yields the following form of Eq. (30) (see appendix B):

$$\dot{\theta}_1 = -2\, d\, J \sin\theta_2 \sin\phi \,, \tag{32a}$$

$$\dot{\theta}_2 = 2\, d\, J \sin\theta_1 \sin\phi \,, \tag{32b}$$

$$\dot{\phi} = 2A - 2\, d\, J(\sin\theta_2 \cot\theta_1 - \sin\theta_1 \cot\theta_2)\cos\phi \,, \tag{32c}$$

where $\phi \equiv \phi_1 - \phi_2$. Here it can be seen that dimensionality enters the equations only by a simple rescaling of the hopping parameter: $J \to d\, J$.

Also, the argument of translational invariance allows one to find a simple expression for $n_{k=0}$:

$$n_{k=0} = n + \tfrac{1}{4} \sin\theta_1 \sin\theta_2 \cos\phi \,. \tag{33}$$

Figure 5 depicts the time evolution of $n_{k=0}$ for the same systems for which the exact solution was presented in Fig. 2. One can clearly see that the mean-field and exact results show a similar shift of the frequency. However, the mean-field solutions exhibit no damping, and hence they are qualitatively incorrect for that quantity.

At this point it is instructive to extract the result for the atomic limit: for $J = 0$, Eq. (32) has the trivial solution $\phi(t) = 2A\, t + \phi(0)$ and $\theta_{1/2}$ constant. Insertion of this result in Eq. (33) immediately reveals the revival time $t_{\mathrm{rev}}^{\mathrm{atom}} = \pi/A$.

Obtaining the solution of the system of Eqs. (32) for finite J is possible by treating them like a classical system (see appendix B). Identification of Hamilton functions and the observation of

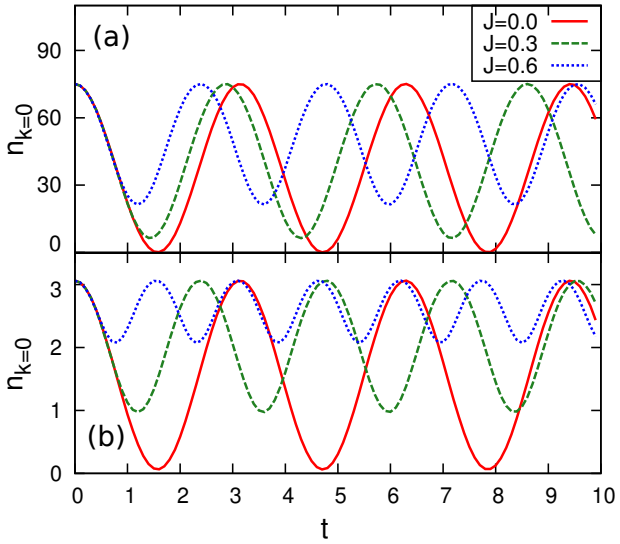

Figure 5: (Color online) Plot of the time evolution of hard-core bosons in a periodic potential in the mean-field approximation for 1D (a) and 2D (b) after a superlattice quench $A_{\rm ini} = 0 \to A_{\rm fin} = 1$ for a system at quarter filling. This is to be compared with the exact results in Fig. 1, where exactly the same system parameters were used.

its trajectories leads to an analytical expression for the period of $n_{\rm k=0}$:

$$t_{\rm rev} = \int_{u_1}^{u_2} {\rm d}u\, f(u), \quad \text{where} \tag{34}$$
$$f(u) = \left\{ d^2 J^2 (1-u^2)[1-(2\gamma-u)^2] - (\mathcal{H}_0' - Au)^2 \right\}^{-\frac{1}{2}}$$

where $\gamma = 2n-1$ and $\mathcal{H}_0' = -4n(1-n)\, d\, J - \gamma A$. A closed expression for the preceding integral exists. However, it is cumbersome and does not provide any apparent information on the functional form of $t_{\rm rev}$ as it depends on the elliptic integral of the first kind. The integral limits u_1 and u_2 are the solutions of $1/f(u) = 0$ that lie within $[-1, 1]$. This requires solving the root of a polynomial of fourth order, which can also be done analytically. The lower boundary u_1 is given by a simple expression: $u_1 = \gamma$. In the case of half filling, also the upper boundary is given by a simple expression: $u_2 = \frac{A}{2dJ}\left(\sqrt{1 + 8d^2J^2/A^2} - 1\right)$.

In Fig. 6, we plot the analytic solution for different dimensions at quarter filling. As mentioned before, dimensionality in the mean-field picture is captured by a simple rescaling of $J \to d\, J$. For comparison, we depict numerical solutions of Eq. (30) as points in the plot. The latter are required for studying the inhomogeneous trapped hard-core boson case and soft-core bosons, for which no analytic solutions are available.

The analytic expression (34) allows us to confirm the numerical finding for the scaling relations of $t_{\rm rev}$ and $n_{k=0}^{\rm rev}$ with respect to the parameters A and J. The proposed scaling for the revival time $t_{\rm rev}(J, A) \equiv t_{\rm rev}(J/A)/A$ does obviously hold for the integrand $f(u)$ in Eq. (34). The fact that for the integration limits one has $u_{1/2}(J, A) \equiv u_{1/2}(J/A)$, proves the proposition for the mean-field case.

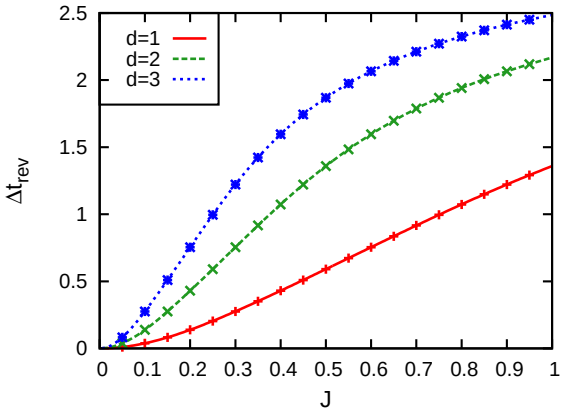

Figure 6: (Color online) Plot of the revival time $\Delta t_{\rm rev} = t_{\rm rev}^{\rm atom} - t_{\rm rev}$ for a system of hard-core bosons in a periodic potential and a superlattice quench $A_{\rm ini} = 0 \to A_{\rm fin} = 1$. $t_{\rm rev}$ is given by the analytic solution Eq. (34). Depicted are results for 1D, 2D, and 3D. The data points are numerical solutions of the set of Eqs. (30).

Furthermore, the evaluation of Eq. (33) leads to the expression

$$n_{k=0} = n - \tfrac{1}{4dJ}(\mathcal{H}_0' + A\cos\theta_1)\,, \tag{35}$$

where one can see, (i) that no damping of $n_{k=0}$ occurs within the mean-field approximation in the hard-core limit and (ii) that $n_{k=0}$ only depends on J/A as found for the numerical solution.

We note also that for the case of half filling and $d\,J = 1$, Eq. (34) yields $t_{\rm rev} \to \infty$, reflecting the fact that the mean-field equations of motion do not predict any oscillations in this case – in contrast to the exact solution. With the absence of damping and the last observation, there are already two deficiencies of the mean-field approximation that we need to keep in mind for the analysis that follows – this makes the comparison to the exact solution an essential duty to ensure one has an idea of the limits of the validity of the mean-field results presented in Sec. 5.

4.2. Exact vs mean-field results

In equilibrium, a detailed comparison between the predictions of the mean-field theory introduced before and exact quantum Monte Carlo simulations for the ground state of hard-core bosons in the presence of a superlattice potential was presented in Refs. [18,19]. The Gutzwiller approach was found to correctly predict the two phases present in the ground state of this model, namely, a superfluid phase for all fillings but $n = 0, 1/2$, and 1 and for $n = 1/2$ below a critical value of A/J and a Mott insulator (a charge density wave) for $n = 1/2$ above a critical value of A/J. However, Gutzwiller mean-field theory was shown to provide a poor estimate of the critical value of A/J for the superfluid-Mott-insulator transition. It overestimated it by around 100% in 2D and a 50% in 3D.

As shown in the previous section, after the quench in the periodic system, the mean-field solution does not exhibit any damping for the amplitude of the oscillation whereas in the exact

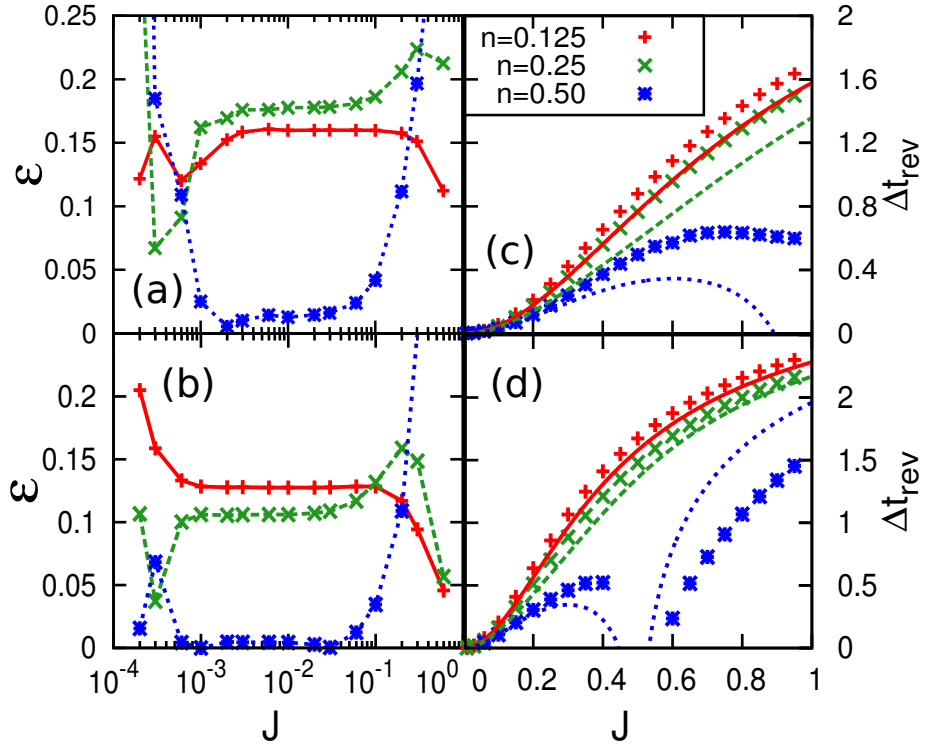

Figure 7: (Color online) Comparison of the mean-field approximation and the exact solution for 1D (a, c), and 2D (b, d). In (a) and (b), we plot the error introduced in (36) on a linear-log scale for the systems presented in Fig. 2. In (c) and (d), we again show the results presented in Fig. 2 but this time on a linear scale together with the mean-field results, where the latter are drawn as lines and were calculated via the analytical solution (34).

solution there obviously is damping. For this reason, we do not study the damping any further. In the remainder of the article we therefore focus on the predictions of mean-field theory for the corrections to the revival time.

In order to be more quantitative, we define the relative deviation of the mean-field approximation from the exact solution by

$$\varepsilon(J) = \frac{\Delta t_{\rm rev}^{\rm ex}(J) - \Delta t_{\rm rev}^{\rm mf}(J)}{\Delta t_{\rm rev}^{\rm ex}(J)} \tag{36}$$

where $\Delta t_{\rm rev}^{\rm ex}(J)$ and $\Delta t_{\rm rev}^{\rm mf}(J)$ are the corrections to the revival time due to a finite value of J for the exact and mean-field solutions, respectively.

In Figs. 7(a) and 7(b), we plot $\varepsilon(J)$ in a linear-log scale vs J. That figure shows an almost constant error over two decades ($10^{-3} \lesssim J \lesssim 10^{-1}$). For $J \lesssim 10^{-3}$ rounding-off errors set in as one starts dealing with numbers $\sim 10^{-10}$; that is, the deviations seen in that region are not to be considered any further. The absolute value in the constant part of the deviation is around 16% for 1D (a) and 11% for 2D (b) for $n = 0.125$ and $n = 0.25$. At half filling, interestingly, the deviation is yet much smaller. In all cases, it is obvious that the mean-field approximation

describes the 2D system better than the 1D case, even though the system size in 1D is one order of magnitude larger than in 2D and mean-field is expected to be more accurate as the system size is increased.

In Figs. 7(c) and 7(d), we present the same results as in Fig. 2 and compare them to the mean-field predictions, but this time in a linear scale. This scale emphasizes the differences between the mean-field results and the exact ones for values of J close to $A = 1$. Once again, it is obvious that the mean-field approximation works better in 2D than in 1D, and that it becomes a very good approximation of the exact results for $n = 0.125$ and $n = 0.25$. We further note the already-mentioned case of $dJ = 1$, which does not yield any revival in the mean-field approximation and therefore $\Delta t_{\rm rev} \to \infty$ as the figures suggests. Interestingly, there is a corresponding anomaly in the exact solution in 2D: there, in a neighborhood of $J = 0.5$, the exact solution does not produce a symmetric peak after the first revival oscillation, which makes it meaningless to determine a value for the revival time – therefore these data points are missing. Finally, Figs. 7(a) and (b) show that at half filling mean-field theory provides the most accurate results for the quadratic region of small values of J, whereas it provides the worse results for large values of J, as seen in (c) and (d).

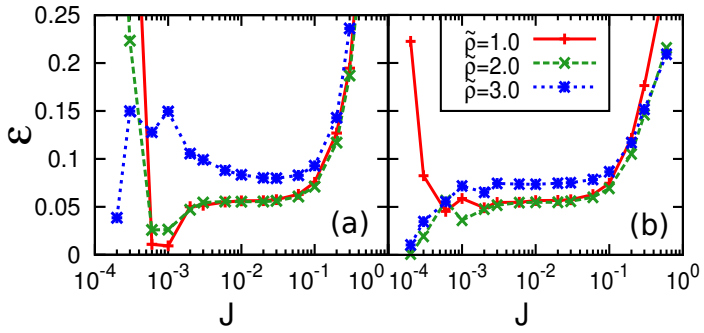

Figure 8: (Color online) Plots of the error (36) for the 1D trapped case presented in Fig. 4 for: (a) quench type (i) keeping the characteristic density constant and (b) quench type (ii) turning off the trap, both presented on a linear-log scale.

Results for $\varepsilon(J)$ in the 1D trapped case are presented in Fig. 8 for the two types of quenches introduced in the previous section: (i) the scenario of a constant characteristic density and (ii) switching off the trapping potential. The behavior is qualitatively the same as just discussed for the homogeneous case of Fig. 7(a). Quantitatively, we find an error $\sim 5\%$, which is in between the values for low and half filling in Fig. 7(a), and is similar for both quench types. Such an intermediate value is expected because the trap causes a density profile with different densities in different regions of the trap.

For the description of experiments, which are of more interest in 3D trapped geometries and very large system sizes, one can expect much smaller errors than the ones in Fig. 8. Therefore, we conclude that the shift of the revival time due to a finite hopping is correctly captured not only qualitatively but also quantitatively by the mean-field approximation described here. This is an interesting finding considering that, in contrast, the description of the evolution of the

amplitude in terms of the mean-field approximation is incorrect even at the qualitative level.

5. Results for soft-core bosons

In Refs. [3, 26] it has already been shown that ultracold bosonic gases in optical lattices can be well described by the bosonic Hubbard model (26). In light of the recent results in Refs. [6, 7] mentioned in the introduction, we note that the interaction constant U and the hopping amplitude J in the Hamiltonian (26) are the effective two-body interaction and one-body hopping, respectively, whose origin is not under discussion here. They may be obtained after multi-orbital renormalization effects are taken into account. Multi-orbital effects may also generate effective higher-body interactions that translate into additional frequencies during the collapse and revival of the matter-wave interference but are not considered here. These effects can be reduced by properly engineering the initial state. We focus on the effect that a finite effective hopping J has on the fist revival of the matter wave.

Collapse and revival oscillations like the ones observed experimentally in Refs. [2,6] have been reproduced in 1D bosonic [27] and fermionic [28] systems by means of numerically exact time-dependent renormalization group techniques. Here we use mean-field theory to study 3D bosonic systems theoretically. Following the results of the previous section, we expect the mean-field predictions for the tunneling-induced correction of the revival time of the value in the atomic limit Δt_{rev} to be close to the exact results.

We proceed in the way introduced in the preceding section. For soft-core bosons, we solve the equations (30) for a cutoff of $n_{\mathrm{c}} = 7$ numerically. This cutoff ensures convergence with respect to the energy expectation value and the momentum distribution, and was successfully employed in Ref. [29] to study the superfluid-Mott-insulator transition. Initially, the system is prepared in the Gutzwiller mean-field ground state of the trapped system at an intermediate interaction $U_{\mathrm{ini}} = 6J_{\mathrm{ini}}$ ($J_{\mathrm{ini}} = 1$ sets our energy scale), which ensures the validity of a one-band model in experiments while the system is still far from the transition to the Mott insulator. Within the mean-field approximation $(U/J)_{\mathrm{crit}} = 34.8$ (for six nearest neighbors) [20, 30, 31]. At time $t = 0$, the on-site interaction is doubled to $U_{\mathrm{fin}} = 12$ and we investigate the collapse and revivals for several values of $J_{\mathrm{fin}} < 1$ (where, as in the section about hard-core bosons, the notation $U_{\mathrm{fin}} \equiv U$ and $J_{\mathrm{fin}} \equiv J$ is used in all unambiguous cases).

Figure 9 depicts the collapse and revival oscillations for the homogeneous case. These predictions, within mean-field theory, correspond to the solution of a single site problem. They clearly exhibit a different functional form when compared to the ones for hard-core bosons in a superlattice potential Fig. 2. Also, not only a shift in the revival time is present but additionally a damping of the amplitude can be observed. We do not consider this damping effect, as we cannot make any statement about the validity of the mean-field approximation for this quantity (see Sec. 4). We note again that the revival time for the interaction quench in the atomic limit is given by $t_{\mathrm{rev}} = 2\pi/U$.

In Fig. 10, we show Δt_{rev} for several densities in the homogeneous case. We observe a linear

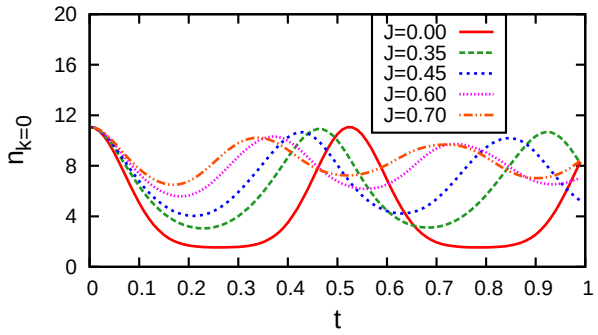

Figure 9: (Color online) Dynamics of the zero momentum peak $n_{k=0}$ vs time t for a system with homogeneous potential and density $n = 1.5$. Time is measured in units of $\hbar/J_{\rm ini}$. These results are derived from the mean-field solution of the time evolution (30) for the Bose-Hubbard model after an interaction quench from $U_{\rm ini} = 6$ to $U_{\rm fin} = 12$. Several final values of the hopping constant J are depicted.

relation emphasized by the fits for data points with $J \leq 0.01$ in the figure. Since soft-core bosons are not subject to particle-hole symmetry, the behavior with increasing density is different from the one observed for hard-core bosons in Fig. 2. The smallest deviation from the atomic limit is no longer reached at half filling; instead, for soft-core bosons we find that it appears for a density $n \sim 0.75$. Except for densities around this value, $\Delta t_{\rm rev}$ is not strongly dependent on the density. With respect to the dependence of $\Delta t_{\rm rev}$ on both parameters J and U, we note that the same scaling as in the hard-core case (with A and U interchanged) holds true: $t_{\rm rev}(J,U) \equiv t_{\rm rev}(J/U)/U$.

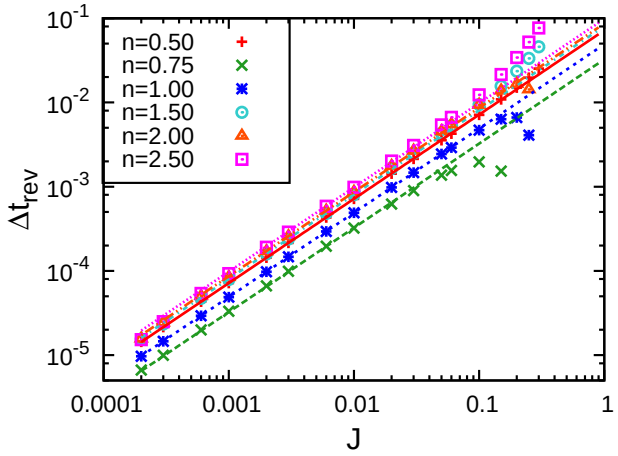

Figure 10: (Color online) Plot of $\Delta t_{\rm rev}$ vs J for soft-core bosons in a homogeneous system and different densities after an interaction quench from $U_{\rm ini} = 6$ to $U_{\rm fin} = 12$. This is done for a single-site system, as the homogeneous result is independent of the system size in the mean-field approximation. Note that the results for different densities lie very close to each other. The linear fits are done for data points with $J \leq 0.01$.

The calculations for the trapped case are more demanding computationally. This is because translational invariance is broken and one has to deal with all the lattice sites in the system.

The results reported here are obtained for a lattice with $L = 30 \times 30 \times 30 = 27000$ sites with $N = 1000$ up to $N = 11000$. As before, finite size effects for our observables of interest are extremely small. As a matter of fact, we found that it would be difficult to distinguish the results reported here from those of a $L = 10^3 = 1000$ system. Again, results are presented for the two quench scenarios analyzed in detail in Sec. 3.3 for hard-core bosons.

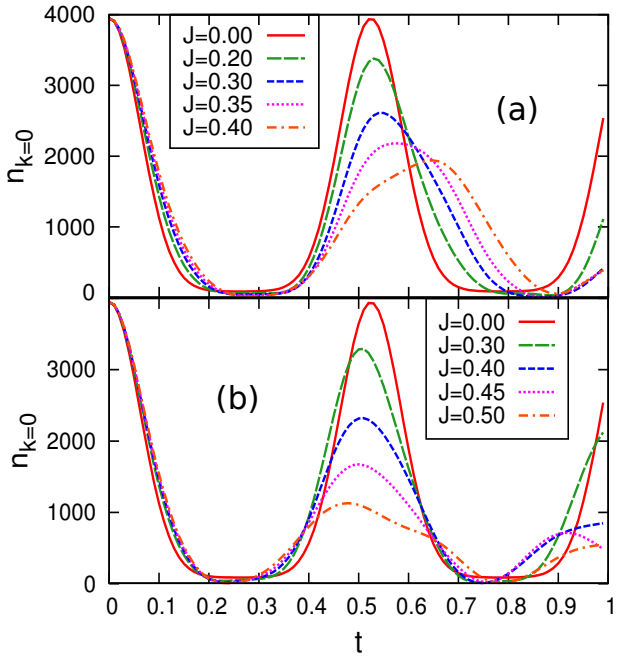

Figure 11: (Color online) Plot of the time evolution of the momentum peak $n_{k=0}$ for ~ 11000 soft-core bosons in a lattice with $L = 30 \times 30 \times 30$ sites for: (a) quench scenario (i), and (b) quench scenario (ii) (see text). The initial state has a characteristic density of $\tilde{\rho} = 39.8$ and an on-site energy $U_{\rm ini} = 6$. At time $t = 0$ the interaction is quenched to $U_{\rm fin} = 12$ and the curvature of the trap is modified according to (i) and (ii).

Results for the time evolution of $n_{k=0}$ in the harmonic trap are shown in Fig. 11 for an initial state with characteristic density $\tilde{\rho} = 39.8$ and the two different quench types: (i) keeping constant the characteristic density and (ii) turning of the trap. Here, we observe an effect that is qualitatively different from the the one seen in the hard-core limit (Fig. 3) and the homogeneous soft-core case, namely, the revival time in the case with finite hopping exceeds the atomic value [Fig. 11(a)]. This effect is only observed in the quench scenario (i) for high characteristic densities. For quench type (ii) the effect is not present for any density [Fig. 11(b)].

In Fig. 12, $\Delta t_{\rm rev}$ is plotted for several values of the characteristic density of the initial state. In Fig. 12(a), results are shown for quench type (i). Note that we account for the fact that the revival time exceeds the atomic limit for high densities by plotting the absolute value of $\Delta t_{\rm rev}$; in particular, $\tilde{\rho} = 23.8$ and $\tilde{\rho} = 39.8$ yield a negative value of $\Delta t_{\rm rev}$. The strong dependence of the results on the characteristic density of the initial system, or equivalently, the initial density in the center of the trap, makes this scenario unsuitable for experimentally probing the values of J after the quench. The experimental uncertainty of the filling in the center of the trap would

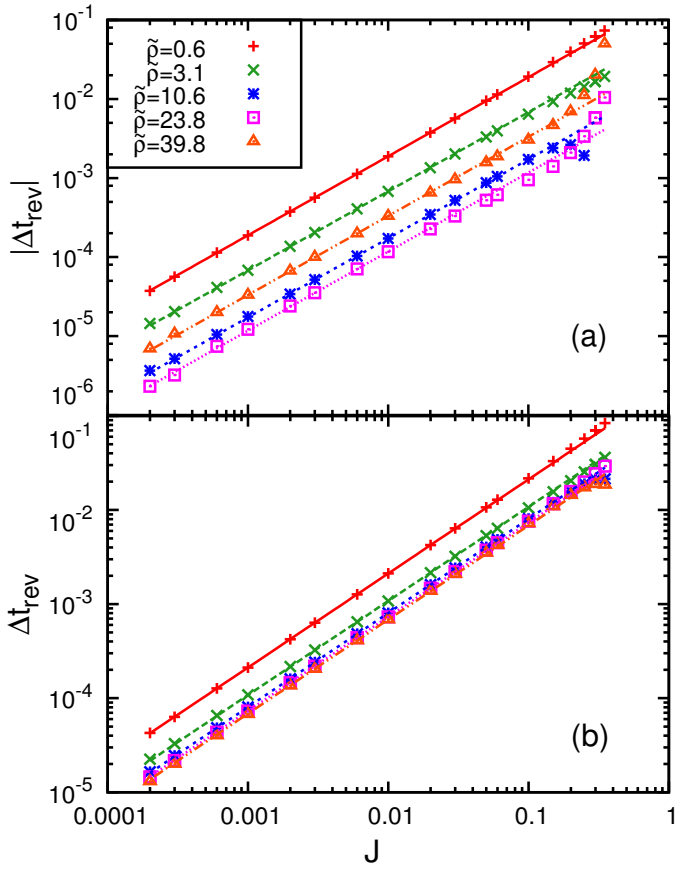

Figure 12: (Color online) Quantum corrections to the revival time ($\Delta t_{\rm rev}$) vs J for the scenarios: (a) keeping the characteristic density constant, and (b) turning of the trap; and an interaction quench $U_{\rm ini} = 6 \rightarrow U_{\rm fin} = 12$. Results are presented for five different initial values of the characteristic density – $\tilde{\rho} = 0.6$, $\tilde{\rho} = 3.1$, $\tilde{\rho} = 10.6$, $\tilde{\rho} = 23.8$, and $\tilde{\rho} = 39.8$ – that correspond to the following values of the density in the middle of the trap: $n_{\rm center} \sim 0.5$, $n_{\rm center} \sim 1.0$, $n_{\rm center} \sim 1.5$, $n_{\rm center} \sim 2.0$ and $n_{\rm center} \sim 2.5$. Note that in (a) $\Delta t_{\rm rev}$ has a negative sign for $\tilde{\rho} = 23.8$ and $\tilde{\rho} = 39.8$; therefore, the absolute value is depicted.

lead to a large uncertainty in determining J.

Scenario (ii) seems to be a good candidate for the latter goal. As depicted in Fig. 12(b), for characteristic densities that are not too small ($\tilde{\rho} \gtrsim 10$) i.e. for densities in the center of the trap that are $n_{\rm center} \gtrsim 1.5$, we observe a weak dependence of the revival time on the characteristic density of the initial state. This is usually fulfilled in experiments like [2]. We also note that the relative deviation $\Delta t'_{\rm rev} = \Delta t_{\rm rev}/t^{\rm atom}_{\rm rev}$ is only one order of magnitude smaller than the normalized hopping parameter J/U, due to the linearity of the relation and a prefactor ~ 0.1. This shows that the described effect is not small and one should be able to measure it in experiments.

Finally, we should mention that we also performed calculations for different values of the interaction constant U before and after the quench. They all exhibited a similar qualitative behavior as depicted in Fig. 12. We therefore stress that our results do not depend on a particular value of U but represent a general behavior that can be reproduced with experimentally relevant

parameters. By comparing experimental results and calculations within mean-field theory, plus using the expected experimental values for U, one could then use experimentally measured values of $\Delta t_{\rm rev}$ to determine the final value of J.

6. Conclusion

We have presented a detailed study of the dependence of collapse and revival properties of the matter-wave interference in lattice boson models on a finite tunneling amplitude after an interaction quench.

We first studied quenches of hard-core bosons on a superlattice potential. For those systems, we presented exact numerical results in 1D and 2D, and compared them with the approximated mean-field solution. Both approaches exhibited the same functional form of the correction to the revival time produced by finite hopping parameters after the quench, with a leading behavior $\sim t^2/A^3$. The mean-field results were also shown to have, as expected, smaller errors in 2D as compared to 1D. Since the largest errors for homogeneous 2D systems were $\sim 10\%$ and for trapped 1D systems $\sim 5\%$ (in contrast to $\sim 17\%$ for the 1D homogeneous case), we expect that in 3D trapped systems, mean-field theory should provide relatively accurate results for the corrections to the revival time.

We then studied interaction quenches in the Bose-Hubbard model in 3D. In this case, our analysis was solely based on the Gutzwiller mean-field theory. We showed that for soft-core bosons the corrections to the revival time in the atomic limit, due to finite values of J after the quench, are $\sim J/U^2$. This is an effect that could be measured experimentally. Given the weak dependence of the correction on the initial density profile, provided the density in the center of the trap is greater than $n = 1.5$, we have proposed that the corrections to the revival time measured experimentally could be used to determine the actual value of J after the quench. The only input one would need is the experimental value of U and the mean-field predictions from calculations similar to the ones presented here.

Appendix

A. Derivation of the "Jaksch Equations"

The Hamiltonian (26) can be transformed as follows

$$\begin{aligned}\hat{H}_{\mathrm{SCB}} &= -J\sum_{\langle ij\rangle}(\hat{a}_i^\dagger\hat{a}_j + \mathrm{H.\,c.}) + \tfrac{U}{2}\sum_i \hat{n}_i(\hat{n}_i-1) + \sum_i \hat{n}_i V_i \\ &= -J\sum_i\sum_{\langle j\rangle_i}\hat{a}_i^\dagger\hat{a}_j + \tfrac{U}{2}\sum_i \hat{n}_i(\hat{n}_i-1) + \sum_i \hat{n}_i V_i \\ &= \sum_i\Big(-J\sum_{\langle j\rangle_i}\hat{a}_i^\dagger\hat{a}_j + \hat{n}_i\big(\tfrac{U}{2}(\hat{n}_i-1)+V_i\big)\Big), \end{aligned} \tag{37}$$

where V_i is a local potential and the sum $\sum_{\langle j\rangle_i}$ denotes summation over a all nearest neighbors j of site i.

First we want to minimize the energy expectation value $\langle\Psi_{\mathrm{MF}}|\hat{H}_{\mathrm{SCB}} - \mu\hat{N}|\Psi_{\mathrm{MF}}\rangle$ with the Gutzwiller product state $|\Psi_{\mathrm{MF}}\rangle = \prod_{i=1}^{L}\sum_{n=0}^{n_c}\alpha_{in}|n\rangle_i$.

For this consider the action of the hopping operator $\hat{a}_i^\dagger\hat{a}_j$ on $|\Psi_{\mathrm{MF}}\rangle$ for $i\neq j$:

$$\begin{aligned}&\hat{a}_i^\dagger\hat{a}_j\prod_{i=1}^{L}\sum_{n=0}^{n_c}\alpha_{in}|n\rangle_i \\ &= \Big(\sum_{n=0}^{n_c-1}\alpha_{in}\sqrt{n+1}|n+1\rangle_i\Big)\Big(\sum_{n=1}^{n_c}\alpha_{jn}\sqrt{n}|n-1\rangle_j\Big)\prod_{l\neq i,j}\sum_{n=0}^{n_c}\alpha_{ln}|n\rangle_l \\ &= \Big(\sum_{n=1}^{n_c}\alpha_{i(n-1)}\sqrt{n}|n\rangle_i\Big)\Big(\sum_{n=0}^{n_c-1}\alpha_{j(n+1)}\sqrt{n+1}|n\rangle_j\Big)\prod_{l\neq ij}\sum_{n=0}^{n_c}\alpha_{ln}|n\rangle_l\end{aligned}$$

Which gives for the evaluation of the action of $\hat{H}_{\mathrm{SCB}}$:

$$\begin{aligned}(\hat{H}_{\mathrm{SCB}}-\mu\hat{N})|\Psi_{\mathrm{MF}}\rangle = \sum_i\Big\{&-J\sum_{\langle j\rangle_i}\Big(\sum_{n=1}^{n_c}\alpha_{i(n-1)}\sqrt{n}|n\rangle_i\Big)\Big(\sum_{n=0}^{n_c-1}\alpha_{j(n+1)}\sqrt{n+1}|n\rangle_j\Big) \\ &+\Big(\sum_{n=0}^{n_c}n\big(\tfrac{U}{2}(n-1)+V_i-\mu\big)\alpha_{in}|n\rangle_i\Big)\Big(\sum_{n=0}^{n_c}\alpha_{jn}|n\rangle_j\Big)\Big\}\prod_{l\neq ij}\sum_{n=0}^{n_c}\alpha_{ln}|n\rangle_l\end{aligned} \tag{38}$$

and therefore for $\langle\Psi_{\rm MF}|\hat{H}_{\rm SCB}-\mu\hat{N}|\Psi_{\rm MF}\rangle$

$$\langle\Psi_{\rm MF}|\hat{H}_{\rm SCB}-\mu\hat{N}|\Psi_{\rm MF}\rangle=\sum_i\Big\{-J\sum_{\langle j\rangle_i}\underbrace{\Big(\sum_{n=1}^{n_{\rm c}}\sqrt{n}\alpha_{i(n-1)}\alpha_{in}^*\Big)}_{\equiv\Phi_i^*}\underbrace{\Big(\sum_{n=0}^{n_{\rm c}-1}\sqrt{n+1}\alpha_{jn}^*\alpha_{j(n+1)}\Big)}_{\equiv\Phi_j}$$
$$+\Big(\sum_{n=0}^{n_{\rm c}}n\big(\tfrac{U}{2}(n-1)+V_i-\mu\big)|\alpha_{in}|^2\Big)\tag{39}$$
$$=\sum_i\Big\{-J\sum_{\langle j\rangle_i}\Phi_i^*\Phi_j-\Big(\sum_{n=0}^{n_{\rm c}}n(\tfrac{U}{2}(n-1)-\mu_i)|\alpha_{in}|^2\Big)\Big\}\tag{40}$$

where $\mu_i=\mu-V_i$.

Making this stationary requires differentiating which is easily done if expression (39) is employed and the appearance of the variable α_{in}^* in the sum over nearest neighbors is carefully counted:

$$\partial_{\alpha_{in}^*}\langle\Psi_{\rm MF}|\hat{H}_{\rm SCB}-\mu\hat{N}|\Psi_{\rm MF}\rangle=0$$
$$\Leftrightarrow -J\sum_{\langle j\rangle_i}\Big(\sqrt{n}\alpha_{i(n-1)}\Phi_j+\sqrt{n+1}\alpha_{i(n+1)}\Phi_j^*\Big)+n\Big(\tfrac{U}{2}(n-1)+V_i-\mu\Big)\alpha_{in}\tag{41}$$

Due to hermiticity the partial derivation with respect to the complex conjugate variable yields the same result.

We further need

$$i\partial_t\prod_{i=1}^{L}\sum_{n=0}^{n_{\rm c}}\alpha_{in}|n\rangle_i=i\sum_i\sum_{n=0}^{n_{\rm c}}\dot{\alpha}_{in}|n\rangle_i\prod_{l\neq i}\sum_{n=0}^{n_{\rm c}}\dot{\alpha_{ln}}|n\rangle_l$$
$$\Rightarrow\langle\Psi_{\rm MF}|i\partial_t|\Psi_{\rm MF}\rangle=i\sum_i\sum_{n=0}^{n_{\rm c}}\alpha_{in}^*\dot{\alpha}_{in}\,.\tag{42}$$

Following the so called time-dependent variational principle [24] we stationarize the Schroedinger equation: with the expressions (41) and (42) the result follows immediately:

$$\partial_{\alpha_{in}^*}\langle\Psi_{\rm MF}|i\partial_t-\hat{H}_{\rm SCB}+\mu\hat{N}|\Psi_{\rm MF}\rangle=0$$
$$\Leftrightarrow i\alpha_{in}=-J\sum_{\langle j\rangle_i}\Big(\sqrt{n}\alpha_{i(n-1)}\Phi_j+\sqrt{n+1}\alpha_{i(n+1)}\Phi_j^*\Big)+n\Big(\tfrac{U}{2}(n-1)+V_i-\mu\Big)\alpha_{in}\,.\tag{43}$$

This is the set of equations (30) we call “Jaksch Equations”.

B. Hard-core bosons in the Gutzwiller approximation

We employ and re-evaluate the expressions just calculated for the general form of the Gutzwiller wave function ansatz (27) for (31) by identification of

$$\alpha_{i0} = \sin\frac{\theta_i}{2}\mathrm{e}^{i\chi_i}, \qquad \alpha_{i1} = \cos\frac{\theta_i}{2}\mathrm{e}^{i\phi_i}\mathrm{e}^{i\chi_i}, \tag{44}$$

which corresponds to a cut-off of $n_c = 1$ in the ansatz for the Gutzwiller wave function.

Let us first give some equilibrium properties of the system in terms of this parametrization (compare [19]). All expectation values are given in terms of the HCB ansatz (31).

B.1. Equilibrium ground state and observables

We have

$$\langle a_j\rangle = \Phi_j = \sum_{n=0}^{n_c-1}\sqrt{n+1}\alpha_{jn}^*\alpha_{j(n+1)} = \sin\frac{\theta_j}{2}\cos\frac{\theta_j}{2}\mathrm{e}^{i\phi_j} = \frac{1}{2}\sin\theta_j\mathrm{e}^{i\phi_j} \tag{45}$$

and

$$\langle n_i\rangle = \sum_{n=1}^{n_c} n\alpha_{in}^*\alpha_{in} = |\alpha_{i1}|^2 = \cos^2\frac{\theta_i}{2} = \frac{1}{2}(\cos\theta_i + 1) \tag{46}$$

which yields when inserted in (39) and using for the kinetic term $-J\sum_i\sum_{\langle j\rangle_i}\Phi_i^*\Phi_j$ the identity $\frac{1}{2}\sum_i\sum_{\langle j\rangle_i}\sin\theta_i\sin\theta_j\mathrm{e}^{i(\phi_j-\phi_i)} = \sum_{\langle ij\rangle}\sin\theta_i\sin\theta_j\cos(\phi_i-\phi_j)$:

$$E = \langle H_{\mathrm{HCB}}\rangle = -\frac{J}{2}\sum_{\langle ij\rangle}\sin\theta_i\sin\theta_j\cos(\phi_i-\phi_j) + \frac{1}{2}\sum_i V_i(1+\cos\theta_i)\,. \tag{47}$$

All following analytical calculations are done for the periodic system (without trap and hence $V = 0$) with only a super lattice present such that the above energy expectation value takes the form

$$\langle\hat{H}_{\mathrm{HCB}} - \mu\hat{N}\rangle = -\frac{J}{2}\sum_{\langle ij\rangle}\sin\theta_i\sin\theta_j\cos(\phi_i-\phi_j) - \frac{1}{2}\sum_i\mu_i(1+\cos\theta_i)\,, \tag{48}$$

where $\mu_i = \mu + (-1)^{\sigma(i)}A$ is the chemical potential modified with the super lattice potential - $\sigma(i)$ makes up for the generalization of the checkerboard lattice to higher than one dimension: $\sigma(i) = 0$ for the even and $\sigma(i) = 1$ for the odd sublattice.

Minimization of this expression yields the ground state. It is trivially clear from a look on (48) that

$$\phi_i = \phi_j \;\forall i,j \tag{49}$$

has to hold true. Differentiating w.r.t. θ_i then yields

$$\mu_i \tan\theta_i = J \sum_{\langle j \rangle_i} \sin\theta_j \,. \tag{50}$$

For the homogeneous system with $\mu_i \equiv \mu$, $\theta_i \equiv \theta$ and therefore $\sum_{\langle j \rangle_i} \sin\theta_j = 2d \sin\theta$ where d is the dimension of the lattice and $2d$ the number of nearest neighbors this simplifies to

$$\cos\theta = \frac{\mu}{2dJ} \,. \tag{51}$$

For the density we get

$$n = \frac{1}{L} \sum_i \langle n_i \rangle = \frac{1}{2L} \sum_i (1 + \cos\theta_i) \,. \tag{52}$$

For the zero momentum occupation number we can use $\langle a_i^\dagger a_j \rangle = \Phi_i^* \Phi_j$ for $i \neq j$ such that we obtain

$$\begin{aligned} n_{k=0} &= \frac{1}{L} \sum_{ij} \langle a_i^\dagger a_j \rangle = \frac{1}{L} \sum_i \langle n_i \rangle + \frac{1}{L} \sum_{i \neq j} \langle a_i^\dagger a_j \rangle & (53) \\ &= \frac{1}{2L} \sum_i (\cos\theta_i + 1) + \frac{1}{4L} \sum_{i \neq j} \sin\theta_i \sin\theta_j \cos(\phi_i - \phi_j) & (54) \\ &= n + \frac{1}{4L} \sum_{i \neq j} \sin\theta_i \sin\theta_j \cos(\phi_i - \phi_j) \,. & (55) \end{aligned}$$

For the periodic 2-site system in d dimensions this simplifies to

$$n_{k=0}^{\text{2site}} = n + \frac{1}{4} \sin\theta_1 \sin\theta_2 \cos(\phi_1 - \phi_2) \,. \tag{56}$$

For the energy of the 2-site system we get when employing (48)

$$\langle \hat{H}_{\text{HCB}} - \mu \hat{N} \rangle^{\text{2site}} = -dJ \sin\theta_1 \sin\theta_2 \cos(\phi_1 - \phi_2) - \frac{1}{2}(\mu + A)(1 + \cos\theta_1) - \frac{1}{2}(\mu - A)(1 + \cos\theta_2) \,. \tag{57}$$

B.2. "Jaksch equations" for hard-core bosons

The Jaksch equations (30) take the following form when inserting the spin state parametrization (44) (compare [15])

$$\begin{aligned} \dot{\theta}_i &= J \sum_{\langle j \rangle_i} \sin\theta_j \sin(\phi_j - \phi_i) \\ \dot{\phi}_i &= \mu_i - J \cot\theta_i \sum_{\langle j \rangle_i} \sin\theta_j \cos(\phi_j - \phi_i) \end{aligned} \tag{58}$$

with an additional equation which determines χ_i, $\dot{\chi}_i = J \cot\frac{\theta_i}{2} \sum_{\langle j \rangle_i} \sin\theta_j \cos(\phi_j - \phi_i)$ which will not further be considered, as χ_i does not appear in any physical quantities.

As justified in the main text, for the periodic case, the system of differential equations reduces to a two-site problem with $\mu_{1/2} = \mu \pm A$ and periodic boundary conditions, such that (58) reads

$$\begin{aligned}
\dot{\theta}_1 &= 2dJ \sin\theta_2 \sin(\phi_2 - \phi_1) \\
\dot{\theta}_2 &= 2dJ \sin\theta_1 \sin(\phi_1 - \phi_2) \\
\dot{\phi}_1 &= \mu + A - 2dJ \cot\theta_1 \sin\theta_2 \cos(\phi_2 - \phi_1) \\
\dot{\phi}_2 &= \mu - A - 2dJ \cot\theta_2 \sin\theta_1 \cos(\phi_1 - \phi_2)
\end{aligned} \tag{59}$$

With the definition of $\phi \equiv \phi_1 - \phi_2$ and subtraction of the last two preceding equations this takes the form (given in the main text and article)

$$\dot{\theta}_1 = -2dJ \sin\theta_2 \sin\phi \tag{60a}$$

$$\dot{\theta}_2 = 2dJ \sin\theta_1 \sin\phi \tag{60b}$$

$$\dot{\phi} = 2A - 2dJ(\cot\theta_1 \sin\theta_2 - \cot\theta_2 \sin\theta_1)\cos\phi \tag{60c}$$

The initial condition employed is the ground state of the homogeneous system (without a superlattice potential present, hence $A = 0$) that has already been calculated ($\phi = 0$ and $\cos\theta = \frac{\mu}{2dJ}$, but we prefer here a parametrization via the density using $n = \frac{1}{2}(1 + \cos\theta)$). Hence this ground state is given by the configuration:

$$\theta_1(t=0) = \theta_2(t=0) = \arccos(\gamma) \quad \text{where} \quad \gamma \equiv 2n - 1 \tag{61a}$$

$$\phi(t=0) = 0\,. \tag{61b}$$

Equations (60) and (61) define an initial value problem with a unique solution.

B.3. Analytic calculation of the revival time

To calculate analytically the revival time for the HCB system in the Gutzwiller approximation, we need to solve the initial value problem (60) and (61). This is done by treating it like a classical system, employing potential and Hamilton functions.

First we note that the quotient $\frac{(60a)}{(60b)}$ (the division is allowed for $\sin\phi \neq 0$ and $\sin\theta_2 \neq 0$ which is fulfilled for the cases we consider) yields the exact (total) differential equation

$$\sin\theta_1 + \sin\theta_2 \frac{\mathrm{d}\theta_1}{\mathrm{d}\theta_2} = 0 \tag{62}$$

with its potential function

$$F(\theta_1, \theta_2) = \cos\theta_1 + \cos\theta_2\,. \tag{63}$$

For exact differential equations, $F(\theta_1(t), \theta_2(t)) \equiv F(t) = F(0)\ \forall t$ holds true. Thus insertion of

the initial condition (61a) yields

$$\theta_2(t) = \arccos(2\gamma - \cos\theta_1(t)) \quad \forall t\,. \tag{64}$$

With this the system (60) can be reduced to two equations. By insertion of (64) and definition of $\theta \equiv \theta_1$ one immediately finds

$$\dot{\theta} = -2dJ\, R(\theta)\, \sin\phi\,, \tag{65a}$$

$$\dot{\phi} = 2A - 2dJ\cos\phi\left(R(\theta)\,\cot\theta - \frac{\sin\theta(2\gamma - \cos\theta)}{R(\theta)}\right), \tag{65b}$$

where $R(\theta) \equiv \sin(\arccos(2\gamma - \cos\theta)) \equiv \sqrt{1-(2\gamma-\cos\theta)^2}$, as $\sin(\arccos(x)) = \sqrt{1-x^2}$. This looks quite horrible, but we remember that they still describe a physical situation where the energy should be conserved being the natural candidate for the Hamilton function of this system of differential equations.

Application of the result (64) in (57) yields for the energy expectation value:

$$\begin{aligned}\mathcal{H}(\theta,\phi) &\equiv \langle \hat{H}_{\mathrm{HCB}} - \mu\hat{N}\rangle \\ &= -dJ\sin\theta\cos\phi R(\theta) - A\cos\theta + C, \qquad (66)\\ &\text{where} \quad C \equiv -(\mu - A)\gamma - A \qquad (67)\end{aligned}$$

The evaluation of the partial derivatives then reads

$$\begin{aligned}\partial_\theta\,\mathcal{H}(\theta,\phi) &= \dot{\phi}\,2\sin\theta\,,\\ \partial_\phi\,\mathcal{H}(\theta,\phi) &= \dot{\theta}\,2\sin\theta\,,\end{aligned}$$

where $\dot{\theta}$ and $\dot{\phi}$ are given by (65). This shows that $\mathcal{H}(\theta,\phi)$ indeed is a Hamilton function for the two coupled equations (65a) and (65b), modified with the Euler multiplier $2\sin\theta$. The Hamilton function does not change with time, therefore

$$\mathcal{H}(t) = \mathcal{H}(t=0) \equiv \mathcal{H}_0. \tag{68}$$

To make use of this property we need to calculate the initial value of $\mathcal{H}$. We consider a super lattice quench. This means that at $t = 0$ a super lattice is ramped up at time scales much faster than the reaction time of the system such that it is still in its ground state at $t = 0$ when the evolution starts. The energy of the system at $t = 0$ is therefore calculated with a super lattice present but with a configuration that is still the ground state of the homogeneous system - we

employ expression (66) and the initial values (61) for θ and ϕ:

$$\begin{aligned}\mathcal{H}_0 &\equiv \mathcal{H}(\theta = \arccos\gamma, \phi = 0) \\ &= -(1-\gamma^2)dJ - \gamma A + C \qquad (69) \\ &= -4n(1-n)dJ - (2n-1)A + C \qquad (70)\end{aligned}$$

For convenience we define

$$\mathcal{H}_0' \equiv \mathcal{H}_0 - C \qquad (71)$$

We can express ϕ in terms of θ by exploiting (68) with (66) inserted

$$\begin{aligned}\mathcal{H}(t) &= \mathcal{H}_0 \\ &\Leftrightarrow \quad -dJ\sin\theta\cos\phi\, R(\theta) - A\cos\theta = \mathcal{H}_0' \qquad (72) \\ &\Leftrightarrow \quad \phi = \arccos\left(\frac{\mathcal{H}_0' + A\cos\theta}{-dJ\sin\theta\, R(\theta)}\right). \qquad (73)\end{aligned}$$

Below we will see that these equations further provide the information about the structure of the orbit of the system (65) necessary to calculate the revival time.

Insertion of (73) into (65a) then yields

$$\dot{\theta} = -2dJ\, R(\theta)\sqrt{1 - \left(\frac{\mathcal{H}_0' + A\cos\theta}{-dJ\sin\theta\, R(\theta)}\right)^2} \qquad (74)$$

where again $\sin(\arccos(x)) = \sqrt{1-x^2}$ was used. This can simply be integrated

$$\begin{aligned}t &= \int_{\theta_0}^{\theta(t)} \frac{\mathrm{d}\theta}{-2dJ\, R(\theta)\sqrt{1 - \left(\frac{\mathcal{H}_0' + A\cos\theta}{-dJ\sin\theta\, R(\theta)}\right)^2}} \qquad (75) \\ &= \int_{\theta_0}^{\theta(t)} \frac{-\mathrm{d}\theta\sin\theta}{2\sqrt{(dJ)^2(1-(2\gamma-\cos\theta)^2)\sin^2\theta - (\mathcal{H}_0' + A\cos\theta)^2}} \qquad (76)\end{aligned}$$

The last integral takes a somewhat prettier form when substituting $u \equiv \cos\theta$:

$$\begin{aligned}t &= \int_{u_0}^{u(t)} \frac{\mathrm{d}u}{2} f(u), \quad \text{where} \qquad (77) \\ f(u) &= \frac{1}{\sqrt{(dJ)^2(1-u^2)(1-(2\gamma-u)^2) - (\mathcal{H}_0' + Au)^2}}\end{aligned}$$

Finally we wish to extract the revival time out of this expression. For this we note that when we insert (64) and (73) in the expression for the zero momentum occupation number (53) we

get a simple expression for $n_{k=0}$ (33):

$$n_{k=0}(t) = n - \frac{1}{4\,d\,J}(\mathcal{H}_0' + A\cos\theta(t))\,. \tag{78}$$

We know from the numerical solution that $n_{k=0}(t)$ is a periodic function. The last equation tells us that $\cos\theta(t)$ defines this periodicity. A full revival is therefore reached if $\cos\theta(t)$ reaches its initial value $\cos\theta_0 = \gamma$. As $\cos\theta(t)$ and $\cos\phi(t)$ are mapped onto each other by (73) they oscillate with the same period (this is as well observed in the numerical solution). Initially we have $\cos\phi_0 = 1$, from the numerical results we further know that $\cos\phi(t)$ oscillates symmetrically around 0 such that a half period is reached when $\cos\phi(t_{\mathrm{rev}}/2) = -\cos\phi_0 = -1$ and a full period when $\cos\phi(t_{\mathrm{rev}}) = \cos\phi_0 = 1$.

By insertion of $\cos\phi(t_{\mathrm{rev}}/2) = -1$ in (73) we can thus determine the value $\theta(t_{\mathrm{rev}/2}) \equiv \theta^*$ of $\theta(t)$ after a half oscillation

$$\begin{aligned} &(73)\\ \Rightarrow \quad &-1 = \frac{\mathcal{H}_0' + A\cos\theta^*}{-dJ\sin\theta^*\,R(\theta^*)}\,. \end{aligned} \tag{79}$$

One immediately observes that finding this value θ^* is equivalent to finding the non-trivial zeros of the denominator of the integrand in expression (75) as - except for the case of half filling - (79) has to be squared to be solved. In this case it is clear that the value of theta after a full oscillation $\theta(t_{\mathrm{rev}}) = \theta_0 = \arccos\gamma$ is another non-trivial solution, as the sign on the left-hand side of (79) does no longer matter. For practical reasons in the following we rather look for the zero of the denominator in the integral expressions based on (75) than talking about the solution of the squared condition (79). Hence, in terms of the integral expression (77) in which the substitution $u \equiv \cos\theta$ was made we can state that the value $u(t_{\mathrm{rev}}/2)$ of $u(t)$ after a half oscillation is given by one of the four zeros of the denominator of $f(u)$. As just explained for θ one solution is $u = u_0 = \gamma$. To identify the correct solution among the other three one uses that it must fulfill $u \in [-1, 1]$ as $u = \cos\theta$. The statement that two of four solutions of $f^{-1}(u) = 0$ are not within $[-1, 1]$ can not rigorously be proven but was numerically tested for many examples. Also $f^{-1}(u) = 0$ can in principle analytically be solved (polynomial of fourth order) but is a cumbersome expression such that we do not give it here. With these considerations we are able to give the final result

$$t_{\mathrm{rev}} = \int_{u_1}^{u_2} \mathrm{d}u\, f(u), \quad \text{where}$$

$$f(u) = \frac{1}{\sqrt{(dJ)^2(1-u^2)(1-(2\gamma-u)^2) - (\mathcal{H}_0' + Au)^2}} \tag{80}$$

$$u_1 \equiv u_0 \equiv \gamma \tag{81}$$

$$u_2 \Leftrightarrow f^{-1}(u_2) = 0 \quad \text{and} \quad u_2 \in [-1, 1] \quad \text{and} \quad u_2 \neq \gamma \tag{82}$$

B.4. Results for half filling

We add the results for the case of half filling ($\mu = 0$, $n = \frac{1}{2}$, $\gamma = 0$) in which the complexity of all expressions reduces a lot. Expressions are denoted with the subscript $_{\mathrm{hf}}$.

The energy becomes

$$\mathcal{H}_{0\mathrm{hf}} = -dJ - A \quad \Rightarrow \quad \mathcal{H}'_{0\mathrm{hf}} = -dJ\,, \tag{83}$$

and

$$R_{\mathrm{hf}}(\theta) = \sqrt{1 - (2\gamma - \cos\theta)^2} = \sin\theta \tag{84}$$

Insertion of these results in the expression for the condition that determines the upper boundary (79) yields

$$-1 = \frac{-dJ + A\cos\theta^*}{-dJ\sin^2\theta^*} \quad \Rightarrow \quad u_2 \equiv \cos\theta^* = \frac{A}{2dJ}\left(\sqrt{1 + 8(\tfrac{dJ}{A})^2} - 1\right) \tag{85}$$

With this and $u_1 = \gamma = 0$ the revival time t_{rev} becomes

$$t_{\mathrm{rev\,hf}} = \int_0^{u_2} \frac{\mathrm{d}u}{\sqrt{(dJ)^2(1-u^2)^2 - (dJ - Au)^2}} \tag{86}$$

B.5. Divergence of the revival time at half filling

The following considerations are based on the general ideas of B. Sciolla on how to treat the preceding integral expression (86). The calculations below were not part of the internship in spring 2010 but added in January 2011.

The revival time for half filling (86) can be written as

$$t_{\mathrm{rev\,hf}} = \frac{1}{dJ}\int_0^{u_2} \frac{\mathrm{d}u}{\sqrt{((1-u^2)^2 - (1 - \frac{A}{dJ}u)^2}}\,. \tag{87}$$

As is noted in the main text, the revival time diverges for $\frac{A}{dJ} = 1$ (where in the main text $A = 1$ is set throughout) in the case of half filling (we note that for half filling in the equilibrium case at $\frac{A}{dJ} = 2$ the transition to the Mott insulator appears). This effect describes a dynamical phase transition in the relaxation behavior of the HCB model after the super-lattice quench. Such a transition has already been described in detail for the Bose-Hubbard model [32].

In the preceding integral expression (87) the divergence becomes apparent when factorizing the denominator of the integrand. Note that $u_2 = 1$ (use (85)) for $\frac{A}{dJ} = 1$ such that (87) formally becomes

$$t_{\mathrm{rev\,hf}} = \frac{1}{dJ}\int_0^1 \frac{\mathrm{d}u}{(1-u)\sqrt{u(u+2)}} \qquad \text{for} \quad \frac{A}{dJ} = 1\,. \tag{88}$$

This expression is clearly divergent due to the behavior of the integrand in the neighborhood of $u = 1$. To extract the nature of the divergence we set $dJ = 1$ and $A = 1 + \varepsilon$ and ε small. The

upper boundary of the integral can now be expanded (use (85)):

$$u_2 = \frac{1+\varepsilon}{2}\left(\sqrt{1+8(\tfrac{1}{1+\varepsilon})^2}-1\right) = 1-\frac{\varepsilon}{3}+\mathcal{O}(\varepsilon^2) \tag{89}$$

Then (87) reads

$$t_{\text{rev hf}} = \int_0^{1-\varepsilon/3+\mathcal{O}(\varepsilon^2)} \frac{\mathrm{d}u}{\sqrt{((1-u^2)^2-(1-(1+\varepsilon)u)^2}} \qquad \text{for} \quad A=1+\varepsilon\,, \quad dJ=1 \tag{90}$$

Expanding the integrand in (90) yields

$$f(u) = \frac{1}{\sqrt{u(2+u)}}\left(\frac{1}{(1-u)}+\frac{\varepsilon}{(1-u)^2(2+u)}\right)+\mathcal{O}(\varepsilon^2) \tag{91}$$

where clearly the second term linear in ε (and also all higher order terms) only yield a finite contribution when evaluated in the integral (90).

We can thus approximate

$$\begin{aligned} t_{\text{rev hf}} &= \int_0^{1-\varepsilon/3} \frac{\mathrm{d}u}{1-u}+\mathcal{O}(1) \qquad \text{for} \quad A=1+\varepsilon\,, \quad dJ=1 \\ &= -\ln(1-u)\big|_0^{1-\varepsilon/3}+\mathcal{O}(1) \\ &= -\ln(\varepsilon)+\mathcal{O}(1)\,. \end{aligned} \tag{92}$$

This is a logarithmic divergence for $\varepsilon \to 0$ known to be characteristic for the dynamical phase transition in the mean field picture [32].

Thanks to

I am grateful to Prof. Marcos Rigol who was a great supervisor, Marcus Kollar who established the contact with him and Prof. Dieter Vollhardt who provided financial support in a very uncomplicated way.

This work was supported by the US Office of Naval Research under Award No. N000140910966 and by the National Science Foundation under Grant No. OCI-0904597.

References

[1] F. A. Wolf, I. Hen, M. Rigol, Phys. Rev. A **82**, 043601 (2010).

[2] M. Greiner, O. Mandel, T. W. Hänsch, and I. Bloch, Nature (London) **419**, 51 (2002).

[3] I. Bloch, J. Dalibard, and Wilhelm Zwerger, Rev. Mod. Phys. **80**, 885 (2008).

[4] E. M. Wright, D. F. Walls, and J. C. Garrison, Phys. Rev. Lett. **77**, 2158 (1996).

[5] A. Imamoglu, M. Lewenstein, and L. You, Phys. Rev. Lett. **78**, 2511 (1997).

[6] S. Will, T. Best, U. Schneider, L. Hackermüller, D. S. Lühmann, and I. Bloch, Nature (London) **465**, 197 (2010).

[7] P. R. Johnson, E. Tiesinga, J. V. Porto, and C. J. Williams, N. J. Phys. **11**, 093022 (2009).

[8] U. R. Fischer and R. Schützhold, Phys. Rev. A **78**, 061603(R) (2008).

[9] M. Rigol and A. Muramatsu, Phys. Rev. Lett. **93**, 230404 (2004); Mod. Phys. Lett. B **19** 861 (2005).

[10] P. Jordan and E. Wigner, Z. Phys. **47**, 631 (1928).

[11] F. F. Assaad, NIC Series Volume 10 Lecture Notes: Quantum Simulations of Complex Many-Body Systems: From Theory to Algorithms p. 111, (2002).

[12] M. Rigol and A. Muramatsu, Phys. Rev. Lett. **94**, 240403 (2005).

[13] M. Rigol, A. Muramatsu, G. G. Batrouni and R. T. Scalettar, Phys. Rev. Lett. **91**, 130403 (2003).

[14] Rigol, M. and Muramatsu, A., Phys. Rev. A **70**, 031603(R) (2004).

[15] Hen, I. and Rigol, M., Phys. Rev. Lett. **105**, 180401 (2010).

[16] V. G. Rousseau, D. P. Arovas, M. Rigol, F. Hébert, G. G. Batrouni, and R. T. Scalettar, Phys. Rev. B **73**, 174516 (2006).

[17] M. Rigol, A. Muramatsu, and M. Olshanii, Phys. Rev. A **74**, 053616 (2006).

[18] I. Hen and M. Rigol, Phys. Rev. B **80**, 134508 (2009).

[19] I. Hen, M. Iskin, and M. Rigol, Phys. Rev. B **81**, 064503 (2010).

[20] M. P. A. Fisher, P. B. Weichman, G. Grinstein, and D. S. Fisher, Phys. Rev. B **40**, 546 (1989).

[21] J. K. Freericks and H. Monien, Phys. Rev. B **53**, 2691 (1996).

[22] B. Capogrosso-Sansone, S. G. Söyler, N. Prokof'ev, and B. Svistunov, Phys. Rev. A **77**, 015602 (2008).

[23] M. Rigol, G. G. Batrouni, V. G. Rousseau, and R. T. Scalettar, Phys. Rev. A **79**, 053605 (2009).

[24] D. Jaksch, V. Venturi, J. I. Cirac, C. J. Williams, and P. Zoller, Phys. Rev. Lett. **89**, 040402 (2002).

[25] S.-K. Ma, *Statistical Mechanics* (World Scientific, Singapore, 1985).

[26] D. Jaksch, C. Bruder, J. I. Cirac, C. W. Gardiner, and P. Zoller, Phys. Rev. Lett. **81**, 3108 (1998).

[27] C. Kollath, A. M. Läuchli, and E.Altman, Phys. Rev. Lett. **98**, 180601 (2007).

[28] S. R. Manmana, S. Wessel, R. M. Noack, and A. Muramatsu, Phys. Rev. Lett. **98**, 210405 (2007).

[29] J. Zakrzewski, Phys. Rev. A **71**, 043601 (2005).

[30] W. Krauth, M. Caffarel, and J.-P. Bouchaud, Phys. Rev. B **45**, 3137 (1992);

[31] K. Sheshadri, H. R. Krishnamurthy, R. Pandit, and T. V. Ramakrishnan, Eurphys. Lett. **22**, 257 (1993).

[32] B. Sciolla and G. Biroli, Phys. Rev. Lett. **105**, 220401 (2010).